Medical Image Analysis 35 (2017) 1–17

Contents lists available at ScienceDirect

Medical Image Analysis

journal homepage: www.elsevier.com/locate/media

Vascular image registration techniques: A living review

Stefan Matl[a,*], Richard Brosig[a], Maximilian Baust[a], Nassir Navab[a,b], Stefanie Demirci[a]

[a] Computer Aided Medical Procedures, Technische Universität München, Munich, Germany
[b] Whiting School of Engineering, Johns Hopkins University, Baltimore MD, US

ARTICLE INFO

Article history:
Received 28 May 2015
Revised 6 May 2016
Accepted 13 May 2016
Available online 25 May 2016

Keywords:
Living review
Medical image registration
Vascular registration techniques
Vascular models

ABSTRACT

Registration of vascular structures is crucial for preoperative planning, intraoperative navigation, and follow-up assessment. Typical applications include, but are not limited to, Trans-catheter Aortic Valve Implantation and monitoring of tumor vasculature or aneurysm growth. In order to achieve the aforementioned goals, a large number of various registration algorithms has been developed. With this review paper we provide a comprehensive overview over the plethora of existing techniques with a particular focus on the suitable classification criteria such as the involved modalities of the employed optimization methods. However, we wish to go beyond a static literature review which is naturally doomed to be outdated after a certain period of time due to the research progress. We augment this review paper with an extendable and interactive database in order to obtain a living review whose currency goes beyond the one of a printed paper. All papers in this database are labeled with one or multiple tags according to 13 carefully defined categories. The classification of all entries can then be visualized as one or multiple trees which are presented via a web-based interactive app (http://livingreview.in.tum.de) allowing the user to choose a unique perspective for literature review. In addition, the user can search the underlying database for specific tags or publications related to vessel registration. Many applications of this framework are conceivable, including the use for getting a general overview on the topic or the utilization by physicians for deciding about the best-suited algorithm for a specific application.

1. Introduction

According to the WHO, cardiovascular diseases (CVDs) "are the number 1 cause of death globally: more people die annually from CVDs than from any other cause" (World Health Organization, 2015). At the same time, this development has brought up large technological achievements enabling faster, safer and more precise medical care. In particular, minimally-invasive procedures have become state-of-the-art interventions and, thereby, increased patient survival rate tremendously. Nowadays, advanced interventional imaging together with smart and intuitive visualization is required in order to allow for image guidance and ensure patient safety throughout the entire procedure. This essentially requires continuous high-level research in medical image processing and visualization.

Enhancing interventional visualization by integrating information extracted from intraoperative and preoperative images of various modalities into one single coordinate frame, is an essential part of image-guided interventions (Peters and Cleary, 2008). Many modalities provide complementary information on tissue as well as deformation changes. Hence the combination can be used to combine respective tissue information, leading to a greater view and a better diagnosis. Image registration between different modalities generally requires identification of feature correspondences in both images. Being present in or near almost all anatomical structures, vessels provide excellent features representing a good basis for multi-modal image registration. In many modalities, vascular structures can be made visible by the use of contrast agent, a radio-opaque dye being injected into the patient's vasculature. Many registration algorithms are based on (contrasted) vessels as intrinsic features, efficiently eliminating any need for extrinsic markers or additional registration features.

Since vessels greatly vary in size and shape and sometimes entire vessel structures are missing, e.g. the majority of the population does not have a complete Circle of Willis (Krabbe-Hartkamp et al., 1998), some authors actually consider vessel trees being a "'fingerprint' of the human anatomy" (Groher et al., 2007) and statistical approaches for registering vessels (Robben et al., 2013) exist only in rare cases. Many vessel registration algorithms

* Corresponding author.
E-mail addresses: stefan.matl@tum.de (S. Matl), r.brosig@tum.de (R. Brosig), maximilian.baust@tum.de (M. Baust), nassir.navab@tum.de (N. Navab), stefanie.demirci@tum.de (S. Demirci).

http://dx.doi.org/10.1016/j.media.2016.05.005

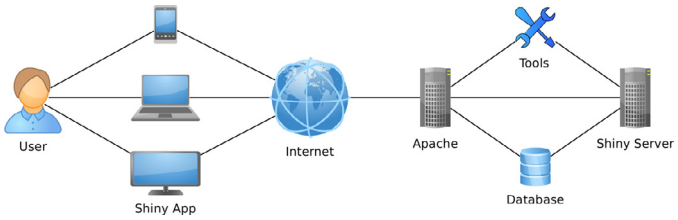

Fig. 1. Overview: The user can access the server via various devices. A Shiny Server is installed on the Apache Server. The Shiny Server can connect to the database containing all tags via SQLite and there are additional tools available for special features. Image created with yEd http://www.yworks.com/en/products/yfiles/yed/.

for different applications and modalities have been developed within the last decades using various cost functions, vascular models and geometric transformations.

1.1. Motivation

With this paper, we aim at surveying medical image registration algorithms that focus on vascular images. These involve algorithms specifically designed for endovascular interventions where vascularity is in the focus of medical care, but also methods that use vascularity as a feature for accurate alignment of various organs. Registration approaches specifically designed for retina imaging are beyond the scope of this paper.

Given the wide range of applications and associated clinical requirements, our survey is intended to provide a general overview to experts as well as novices to the field, adaptive to the respective special intentions. Hence, instead of defining a strict categorization scheme (Markelj et al., 2012), we present an interactive tool visualizing a representation of the review according to 13 defined categories, each describing a certain characteristic of vessel registration algorithms using a specific set of labels.

1.2. Contributions

Providing a comprehensive overview on techniques for the registration of vascular structures is not the only goal of this paper. We also wish to augment the presented survey with an extendable database and interactive visualization making this review a *living* one: While the printed paper serves as a classical review paper as well as a guideline of how to use the associated visualization, the database itself features the following advantages:

1. New papers, categories and tags can be easily added to this database by submitting an extension request[1].
2. Featuring a browser-based front-end, the database can be accessed from any mobile or stationary device, cf. Fig. 1.
3. The user can interactively categorize all entries in a hierarchical manner using tags, such as modality or optimization strategy, as described in Section 2. This yields a tree where the root node represents all entries and the nodes of the next levels represent an instantiation of the respective category as depicted in Fig. 3.

We strongly believe that this proposed combination of a classical review paper and an extendable web-based database is well suited to account for the continuous progress in medical image computing and computer assisted interventions. Thus, we also hope that this work serves as a blueprint for other database-augmented review papers.

In the remainder of this paper, we introduce our classification scheme and visualization, give an overview of existing vascular registration approaches and discuss our results.

[1] Supervision required in order to prevent fraud.

2. Classification scheme

A popular and widely used classification scheme for medical image registration has been proposed by Maintz and Viergever (1998). This already covers many different categories, including dimensionality of input images, nature of a transformation, optimization procedure, necessary (manual) interaction, used modalities, and the subject (nature of registration) and object (application) of a registration method. For a recent and general review on medical image registration, employing this scheme, we refer the interested reader to Markelj et al. (2012). Since the focus of this paper is on vessel registration, we have adapted that scheme and use a modified set of categories to better account for the peculiarities of vessel registration techniques.

2.1. Differences to existing classification schemes

All methods discussed in this paper solely rely on vessels for the registration and do not require any extrinsic basis such as fiducials and stereotactic frames. Therefore, the nature of registration basis is intrinsic in all cases and a corresponding category for classifying approaches into extrinsic or intrinsic does not provide additional information.

Some algorithms also require user interaction, such as supervision of the output, definition of regions of interest or manual selection of corresponding landmarks. However, the clinical feasibility of user interaction significantly depends on the application, i.e. pre- or postoperative vs. intraoperative procedures. Moreover, contemporary computational possibilities differ a lot from a typical setup used decades ago and therefore many semi-automatic pre-processing steps such as segmentation of vascular structures may require less or even no manual interaction anymore. Hence, assessing the required level of manual interaction depends on the environment and the desired use of a certain algorithm. We thus found an evaluation w.r.t. user interaction very subjective and have not considered such a category.

In a similar way, evaluating the runtime of algorithms does not provide much information for the user, unless all algorithms are tested with the same hardware on the very same datasets. Consequently, subjective categories and those that do not provide an additional differentiation of the data are not included in our classification scheme.

The vast majority of algorithms are designed for specific modalities only, since they target particular medical applications or use the characteristic appearance of vessels for segmentation and registration. Since performed validation strategies vary a lot, we decided to also categorize algorithms according to their technological readiness and indicate synthetic tests, phantom studies and comprehensive clinical evaluations.

2.2. Selected categories

The following paragraphs provide a general overview describing all 13 proposed categories and tags associated to each category. For many tags there is a common acronym presented in brackets, which is mainly used for visualization as explained in Section 3. Words and acronyms belonging to the same section are written in italic letters to differentiate them from tags of other categories. Some categories contain hierarchies.

2.2.1. Application

Here, we aim to differentiate certain anatomical regions (of interest), a particular organ, or specific medical procedures. If an approach is labeled with a procedure, it is usually assigned a tag with the particular anatomical region of interest or organ in

addition. Procedures are *Endovascular Aortic Repair (EVAR), Transcatheter Aortic Valve Implantation (TAVI)* and *Transjugular Intrahepatic Portosystemic Shunt formation (TIPS)*. Other related tags are *aorta, aortic valve, head, heart, liver*, and *animal* in case of animal experiments.

2.2.2. Cost function

Cost function defines the actual matching function that is used for alignment. This is usually referred to as similarity measurement for intensity-based registration and as distance measurement for feature-based approaches. For a more compact and general representation, we have adopted the term cost function as general terminology from the optimization theory field. A wide range of cost functions is tagged in a hierarchical manner. *Euclidean distance* and *geodesic distance* are more precise tags and belong to the group *distance-based. Gradient Difference (GD)* and *Gradient Correlation (GC)* are two *gradient-based* cost functions, *Sum of Absolute Differences (SAD)* and *Sum of Squared Differences (SSD)* are *difference-based* tags and *Cross Correlation (CC)* or the special case of *Normalized Cross Correlation (NCC)* as well as *Local Correlation (LC)* are *correlation-based*.

Additional tags are *Fourier-based, Entropy of Difference (EntD)* (Buzug et al., 1996; 1997), *Mutual Information (MI)* (Wells et al., 1996), (Maes et al., 1997), *Entropy Correlation Coefficient (ECC)* (Astola and Virtanen, 1982), the patch-based measurement *Pattern Intensity (PI)* (Weese et al., 1997) or *graph matching*. A more detailed comparison of *NCC, EntD, MI, GC, PI* and *GD* is given by Penney et al. (1998). Finally, many publications describe an additional cost function, simply optimizing the sum of intensities in a target image at projected points or areas. Since no common name is used for that cost function, we define our very own tag *Target Intensity Sum (TIS)*.

2.2.3. Dimensionality

Dimensionality refers to a single modality (mono-modal registration) or to a combination of the dimensions of multiple input modalities (multi-modal registration). A *t* indicates an image sequence. Used tags are *2D to 2D (2D-2D), 3D to 2D (3D-2D), 3D to 3D (3D-3D), biplane to 3D (2x2D-3D), 2D time sequence (2D+t), 2D time sequence to 3D (2D+t-3D), biplane time sequence (2x2D+t)* and *3D time sequence to 2D time sequence (3D+t-2D+t)*. Although the term 2D-3D registration is commonly used in the literature, we follow the terminology of Markelj et al. and use the term 3D-2D registration instead to express that “the 3D image is transformed to achieve the best possible correspondence with the 2D image(s)” (Markelj et al., 2012).

2.2.4. Encoding function

Initially, we used this category to differentiate implicit and explicit encoding functions. Comparing input images by directly using an intensity-based cost function results in an implicit encoding function. If there is a specific representation of the vascular tree or its parts, then this can be called an explicit representation. Bifurcation points, centerline points, a graph or a curve are some examples of an explicit encoding function. However, we intend to make a difference between segmented or extracted representations and those working with raw or filtered images. Inspired by a categorization proposed by Lesage et al. (2009), we differentiate between *appearance* and *geometry*. Raw and filtered images, fuzzy segmentations and similar representations of the vascular tree directly encode the characteristic *appearance* of vessels in medical images. In contrast, most explicit representations are tagged with *geometry*. Binary level sets, which can be seen as an implicit representation, are also tagged with *geometry*, since corresponding centerlines can be immediately extracted by selecting a certain subset only. Sometimes the input is not defined explicitly and the reader can only assume the underlying representation used for registration. As a leading indication supporting the differentiation of *appearance* and *geometry* it should be noted that once features are extracted or a sharply thresholded segmentation of the vascular tree is performed, the representation is most likely based on the underlying *geometry*. A comprehensive survey on various models describing vascularity can be found in Lesage et al. (2009).

2.2.5. Geometry representation

This category can be considered a subcategory of the category Encoding Function, describing those representations tagged with geometry. Whenever vascular structures are not encoded by its appearance, a certain geometry is used. This is also valid if the encoding function is a binary segmentation of the (original) volume. The reason for this categorization is that for a projection of the vessel model it is not relevant whether only points of a graph or all points occupying the segmented voxels have to be projected. In this case, we use the label *volume*.

We further distinguish between point-based, graph-based and curve-based representations. In contrast to point-based representations, graph- and curve-based representations feature a spatial ordering, such as the connectivity given by the neighborhood of a graph. Thus it is important to note that:

1. We always consider discretized curves as graphs, and only use the tag *curves* in case the representation is continuous and allows for a re-sampling of the curve for instance.
2. Both *bifurcation points* and *centerline points* are often combined with additional information other than the position of the point, e.g. the radius of virtual spheres that model the vascular boundaries.
3. Many authors name *curves* or the use of a *graph*, but the actual registration algorithm uses a discrete sampled version or does not employ the spatial connectivity, meaning that *centerline points* is the correct description.

An example for the third observation are algorithms based on the ICP method which will most likely use *centerline points* without any kind of neighborhood or connectivity.

Sometime a mesh is overlaid on a registered image for visual inspection or additional guidance. However, the tag *polygon mesh* only refers to a mesh guiding the registration process, e.g. if the (polygon) mesh is used to render the DRR on the GPU.

2.2.6. Global geometric transformation

An optical registration of vascular structures often requires the optimization of a transformation in order to adjust for scale, rotation as well as local deformations. Most algorithms use a *rigid* global transformation and assume the intrinsic camera model (projective transformation) to be fixed. In contrast to *rigid* transformations, an *affine* transformation allows for additional deformations like shearing, which means that angles are not preserved for instance. All *rigid* transformations form a subset of the *affine* transformation space. In contrast to global *rigid* and *affine* transformations, deformable transformations involve a local deformation, assuming the global transformation to be fixed and optimizing local deformations. In this case, we tag the respective method with *static* and indicate respective local transformations using the category local deformation model (cf. Section 2.2.8). Algorithms can perform both a global and a local deformation, hence the tag *static* can be combined with other tags.

2.2.7. Image representation

Intensity-based approaches largely use an *image-image* representation, meaning that both images are presented as raw data, although they might be filtered. Unlike intensity-based algorithms, a

model-model representation uses features extracted from both images. Combining both options leads to a third group called *model-image* representation. This is common for hybrid approaches as explained in Section 2.2.11.

2.2.8. Local deformation model

In contrast to a global geometric transformation (cf. Section 2.2.6), a local deformation model accounts for local deformations of vascular structures induced by breathing and organ motion and surgical or interventional instruments such as guide wires and catheters. Examples for local deformation models are *B-splines, thin plate splines (TPS)* or more generally *displacement field*. It is important to note that *B-splines* and *thin plate splines* also refer to a certain kind of regularization, because they define the function space in which the sought deformation field lies. As a consequence, we also introduce the tags *length preservation* and *smoothness* in order to account for other popular regularization strategies. The remaining tags indicate a *linear* or a *planispheric* transformation, *spherical harmonics* or a *Fourier decomposition*.

2.2.9. Modality

A wide range of modalities is tagged. For a better differentiation, modalities are presented in groups.

The largest group is *contrasted X-Ray Angiography* consisting of *Computed Tomography Angiography (CTA), Rotational Angiography (RA), Digital Subtraction Angiography (DSA)* and *X-Ray Angiography (XA). CTA* and *RA* refer to a 3D image and *DSA* as well as *XA* to a 2D image. However, there are exceptions and *DSA* can also mean 3D *DSA*. The exact dimension is always inferred from the category dimensionality in Section 2.2.3.

Another group is given by *non-contrasted X-Ray*. 3D *Cone Beam Computed Tomography (CBCT)* and a common 2D *X-Ray* are parts of that group. Compared to *RA, CBCT* is a *non-contrasted X-Ray*.

The third group is *Magnetic Resonance Image (MRI)*. If contrast agent is injected in order to enhance vascular structures, it is called *Magnetic Resonance Angiography (MRA)*. For *Time of Flight MRA (ToF-MRA)* and *Phase Contrast MRA (PC-MRA)*, it is possible to visualize flow within vessels, without the need to administer contrast. These modalities are commonly 3D.

Additional modalities play a smaller role in the database. *Ultrasound (US), Doppler Ultrasound (D-US)* and *Intravascular Ultrasound (IVUS)* are grouped as *US* and are used for 2D and 3D imaging. Finally, there is also *Optical Coherence Tomography (OCT)*.

The tag *model* obviously does not refer to a single modality. It is used for a few publications taking a *model* rather than a modality as input or if authors do not name the exact modality, but argue that every model can be used to achieve that registration. Consequently, a *model* has to be created before the registration, and all approaches tagged with *model* use a preoperatively acquired *model* where manual adjustments could be made.

2.2.10. Optimization

This category covers a huge number of additional tags describing the overall optimization of an algorithm. At first, we introduce the two groups *derivative-free* and *derivative-based* optimization in order to indicate whether a method requires the (analytical or numerical) computation of derivatives. This categorization is of great importance as computing derivatives for certain cost functions can be quite involved.

Additional tags within these two groups are introduced specifying the particular optimization method – *derivative-free* approaches are for instance *Brent*'s method (Brent, 1971) (also known as Brent–Dekker), *Powell*'s method (Powell, 1964) (Powell's conjugate direction method), *Nelder-Mead* method (Nelder and Mead, 1965) (also known as Downhill-Simplex), *greedy search, best neighbor, hill-climbing, bobyqa, cobyla* and *subplex* or a *direct* optimization. In contrast to this, *derivative-based* methods are *Newton*'s method, *Gauss-Newton, gradient descent*, the *Broyden–Fletcher–Goldfarb–Shanno (BFGS)* algorithm which approximates *Newton*'s method, *nonlinear conjugate gradient (nonlinear CG)* or *fminunc*.

The next group describes *probabilistic/stochastic* approaches, it includes tags for an *Oriented Gaussian Mixture Model (OGMM)* or *Weighted Gaussian Mixture Model (WGMM), Monte Carlo* sampling and the use of a *Kalman filter*.

If intensity-based measurements are calculated, the *multi-level* tag indicates multi-resolution. The more general description *multi-level* can also be applied to feature-based approaches, e.g. by continuously raising the sampling frequency of centerline points or by using a subset of a point cloud and gradually increasing that set during registration. Furthermore, the tag *graphics processing unit (GPU)* is mainly used for optimization of Digitally Reconstructed Radiograph (DRR) generation, but the intention is to tag any computation optimized for the GPU. More tags involve *least squares* including *least trimmed squares, dynamic programming (DP)* or an *integral image*. The latter term is also known as summed area table (Crow, 1984) and can be used to efficiently calculate the sum of any rectangular subregion in an image.

2.2.11. Registration basis

This category is closely related to Section 2.2.7 and Section 2.2.2 and defines the nature of values that are compared to each other during the matching process. An *intensity-based* registration basis refers to using intensity values of input images for calculating the cost function. In contrast, *feature-based* approaches model features extracted from input images. While the tag model-based may be a more appropriate terminology to describe these sort of approaches, the term *feature-based* is most commonly used in literature and we adapted this throughout the entire review. In addition, many of these models directly relate to geometric feature descriptors encoding the vascular tree and will in many cases have a geometry representation like centerline points or a graph. Features do not have to be matched to specific vascular geometry, e.g. wavelet coefficient representations could be classified as *feature-based*, although vessels are not represented explicitly. A *hybrid* algorithm utilizes both intensities and extracted features, thus combining those tags. If *hybrid* is used, then *intensity-based* and *feature-based* are not listed in addition.

2.2.12. Subject

In contrast to *intrasubject* registrations matching different images of the same subject (e.g. patient, phantom, animal), *intersubject* methods are not focusing on a single patient anymore, but use input from many individual registrations, e.g. by accessing a preoperatively computed atlas.

2.2.13. Validation

As part of the publication requisites, most algorithms are substantially validated after implementation. Here, different validation scenarios including *synthetic, phantom* and *clinical* data are common. The advantage of *synthetic* data is that the exact deformation (ground truth) is usually known, hence evaluating the results is simple. Moreover, synthetic data can be created if *clinical* data are not available or the algorithm needs more tests before a *clinical* evaluation. Both *phantom* and *clinical* data should be created with a real imaging device and hence, contain acquisition noise or even artifacts. For creating a *phantom* data set, no patients are needed. A *clinical* validation is advisable if *synthetic* and *phantom* tests have been conducted. The main idea of *clinical* tests is further evaluation for real applications with a focus on typical *clinical* use. It is always a good idea to include physicians in *clinical* validation when interpreting the results. There are drawbacks of real tests, mainly the

unknown ground truth of the deformation and the general availability of *clinical* data. Performing an actual test case with patients for the sole purpose of evaluation is not required and validation on *clinical* data can be performed with existing data acquired in the past. A single *clinical* test is not necessarily better or more important than its *synthetic* counterpart, especially if many different *synthetic* examples are used. In fact, by performing a combination of *clinical, phantom* and *synthetic* tests, the evaluation can become much more meaningful.

Some data sets should not be altered or mixed. Testing a 3D-2D registration with *clinical* CTA and a second *synthetic* data set as input or using an extracted vessel model and applying artificial deformations makes the whole test case *synthetic*. If a vessel tree is extracted from a *clinical* MRA, deformed according to a known natural deformation and is then projected by rendering a DRR to simulate a *clinical* DSA, the rendering might not share the same distribution of contrast agent, irregularities in X-Ray attenuation, turbulences within the vasculature or have medical instruments occluding the vessel tree and consequently it can be considered as *synthetic*. Nevertheless, using statistical methods for rendering or adding random noise can greatly enhance the results of *synthetic* tests.

3. Interactive visualization

We have introduced our classification scheme consisting of 13 selected categories. Using such a scheme to review existing literature about vessel registration results in a multidimensional description of each algorithm. One can start a differentiation by choosing a first category to separate algorithms. Then a complete description with respect to that category can be given before continuing with the next one. However, this will not combine the information of multiple categories as attributes of each algorithm will be spread over the description. Another way would be giving a hierarchical review, where a continuous differentiation of literature takes place. Similar to the first approach, it is not possible to assign the same weight to each category, i.e. differentiation will always start with a single category only. Moreover, depending on the reader's personal preferences a particular discrimination might be rather intuitive or not of any use at all. To overcome some of these problems, this section covers the concept and the implementation of our visualization.

3.1. Concept

The idea is to provide the user with a framework for visualizing the attributes of each algorithm in a tree. Unlike the conventional, text-based summary of existing literature, a visual representation creates a simple and intuitive interface allowing the user to recognize relations between algorithms and quickly spot unique approaches. The classification of all algorithms is presented in a web-based interactive app allowing the user to choose a unique perspective for visualization of the data in a tree and perform minor data mining on it. Furthermore, a web-based visualization is easily accessible from almost everywhere.

The presentation of single algorithms in the context of a large tree allows the user to differentiate algorithms based on single tags and get a better understanding of their similarities by comparing them to neighbors in the tree. In addition, the user can search the underlying database for specific tags or single publications related to vessel registration. Many additional features are used, the user can hover over tree nodes to get more information or click on leaves for being forwarded to the publication's website. Our visualization does not demand a certain differentiation and users can create their individual trees according to their specific needs.

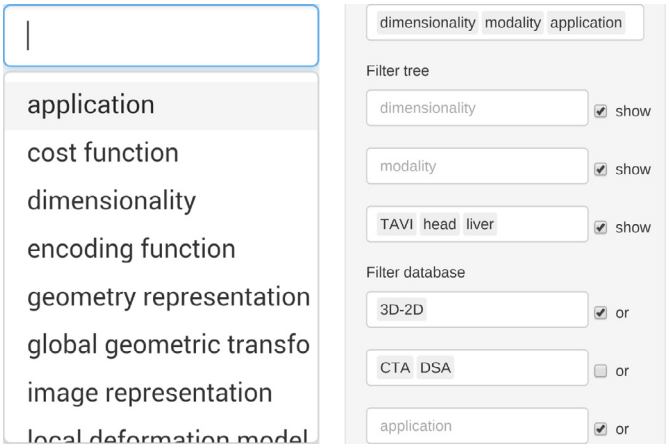

Fig. 2. Interactive website: Screenshot of our website using Chromium V41.

3.2. Implementation

The web-based visualization[2] builds upon Shiny[3], a framework based on the R programming language[4] developed by RStudio[5]. Shiny is an Open Source R package for building web applications using R. Those web applications are called Shiny Apps and on the client side the R source code is replaced by Hypertext Markup Language (HTML) and JavaScript (JS). The framework aims at creating a fast and responsive interface, where elements of the website are automatically updated. For hosting Shiny Apps, a Shiny Server is needed. We opted for the Open Source Edition of Shiny Server[6].

A basic setup is depicted in Fig. 1 showing the main components. The App visualizes the tags in a tree and the user can perform minor data mining on it by selecting categories which are used to sort the tree. Each layer of the tree belongs to one category, some categories contain hierarchies and every leaf represents an algorithm. Since the number of tags used within each category is not constrained, algorithms tagged with multiple tags of a certain category will be represented with several leafs in the tree. Hovering over such a leaf will then highlight corresponding leafs belonging to the same paper. The user can also search for single tags. The tree is visualized with Scalable Vector Graphics (SVG)[7].

Part of our input interface is depicted in Fig. 2. The idea is to let the user choose single categories (from all 13 available ones) and assign each level of the tree to exactly one category. For each selected category, two more input fields are created for filtering using specific tags. One input field allows filtering the database, i.e. only papers associated with the used tag are queried, and the other one allows filtering the tree, i.e. only subtrees related to a respective tag are shown. Every change of input values triggers an update on the server side, a specific database query is issued and the resulting dataframe is converted to a tree structure. A corresponding SVG code containing the tree is send back to the client and a new tree will be rendered in the browser. In order to provide users with more background information for performing a personal evaluation, algorithms can be filtered by their publication type (e.g. journal or proceedings) and date. There are many more additional options and different layouts available. The main screen of our website is depicted in Fig. 3.

[2] http://livingreview.in.tum.de.
[3] http://www.shiny.rstudio.com/.
[4] http://www.r-project.org/.
[5] http://www.rstudio.com/.
[6] http://www.rstudio.com/products/shiny/shiny-server/.
[7] https://www.w3.org/Graphics/SVG/.

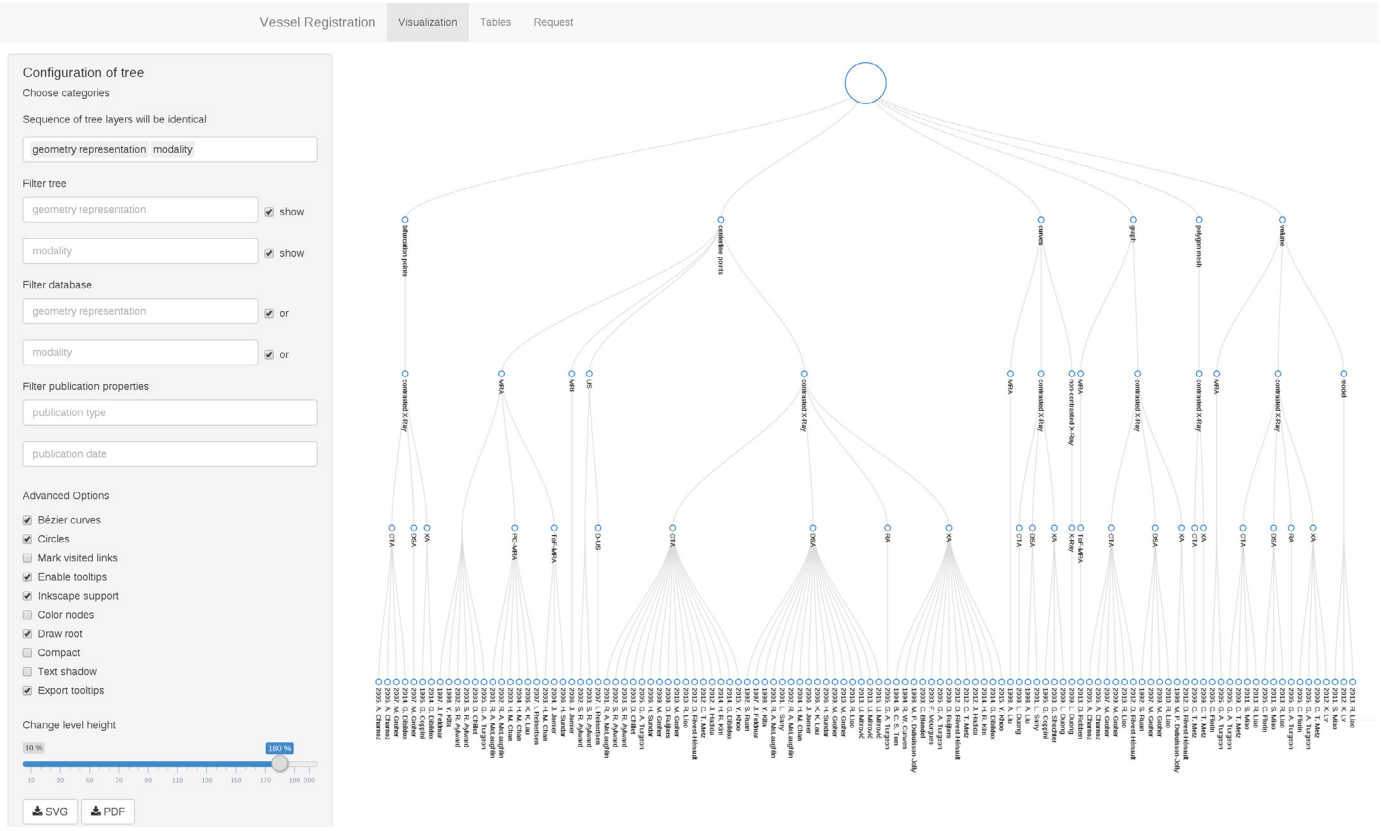

Fig. 3. Input: Entering multiple categories in a row and constraining single categories by using tags.

4. A Review on vessel registration algorithms

This section gives a detailed overview of existing vascular registration approaches. Due to the large variety of different categories and even more tags, we aimed at finding suitable combinations of related categories and present a large part of the review using four large sections. First, we take a close look at registration basis, used cost function and underlying representation of the vascular tree. The next section mostly covers intended applications and both global and local deformations, followed by a section about image data including modality, dimensionality and performed validation. The last section reviews algorithms with respect to their optimization.

To a large amount, these sections are distinct. The intention here is that not every reader is interested in all four of them, but may have a specific purpose or interest. We have identified four potential user groups distinct in their particular interest (see Fig. 4 for a graphical outline). While Section 4.1 focuses on categories registration basis, cost function and image representation and is therefore certainly more suitable for users being interested in fundamental research on vessel registration approaches, Section 4.2 on application and deformation is more likely to be read by engineers or students interested to find a solution for specific application or clinical challenge. Section 4.3 clearly targets clinicians and clinical engineers interested to build up innovation with a high technology-readiness level. If the intention is fundamental research or developing a new and better algorithm, then representations of vessels, details about used cost functions and employed optimizations in Section 4.4 should be relevant.

This review structure follows our concept of individual review. Our intention is to provide more than a fixed scheme and we augment our description with figures giving an immediate overview for a better differentiation. For each figure, the caption includes an ordered list with all categories and tags used to create the respective tree visualization on our website.

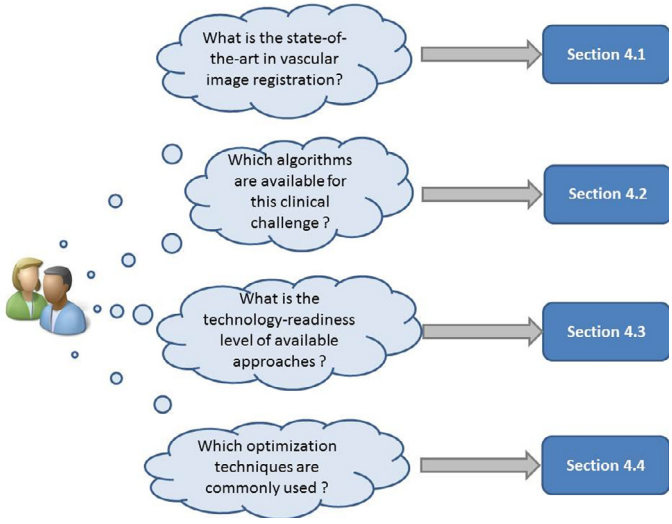

Fig. 4. Graphical Outline of Section 4: User guidelines on how to read Section 4 with a specific purpose.

4.1. Registration basis, cost function and image representation

Image registration involves optimization of a measure assessing the quality of the current geometric transformation. The nature of

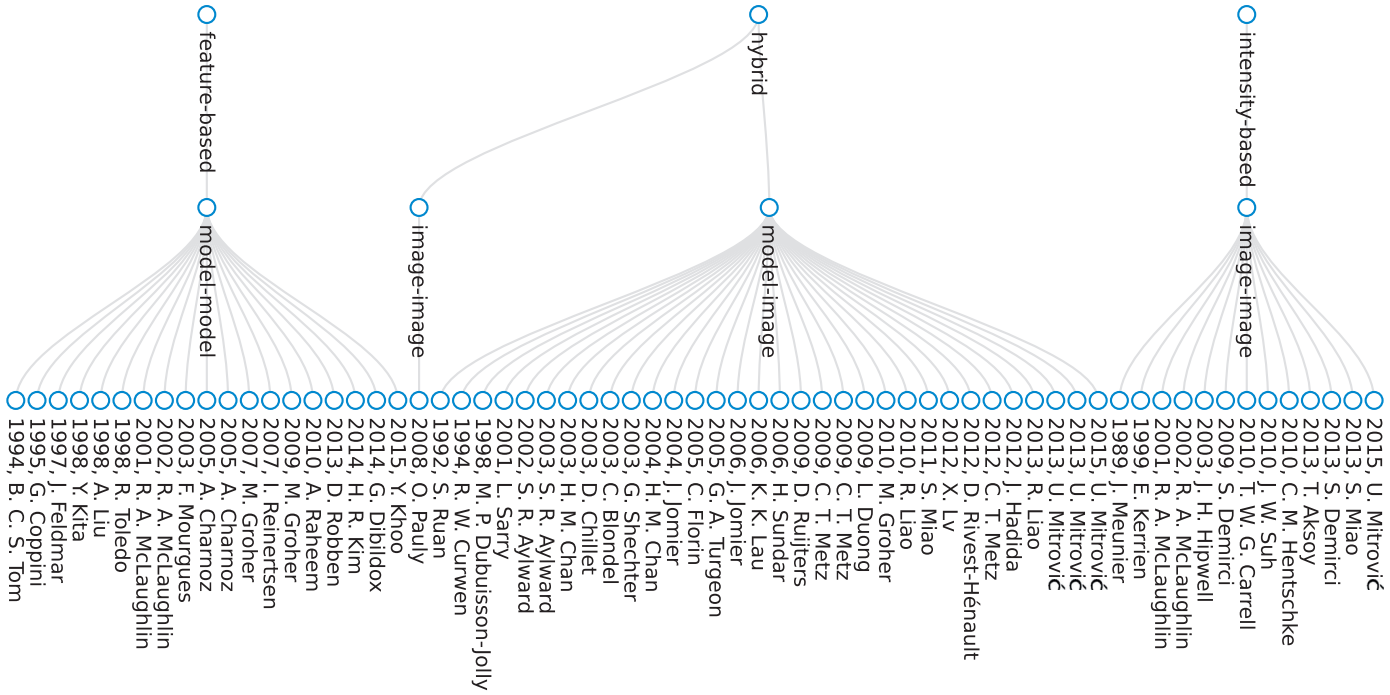

Fig. 5. Image representation: Categories: registration basis, image representation. Tags: none.

this quality measure is referred to as registration basis and is depicted in Fig. 5. Feature-based algorithms (Charnoz et al., 2005a; 2005b; Coppini et al., 1995; Dibildox et al., 2014; Feldmar et al., 1997; Groher et al., 2007; 2009; Khoo and Kapoor, 2015; Kim et al., 2014; Kita et al., 1998; Liu et al., 1998; McLaughlin et al., 2001; 2002; 2005; Mourgues et al., 2003; Raheem et al., 2010; Reinertsen et al., 2007; Robben et al., 2013; Toledo et al., 1998; Tom et al., 1994) mainly use distance-based measures on features extracted from one or both input images to be aligned. Intensity-based algorithms (Aksoy et al., 2013; Carrell et al., 2010; Demirci et al., 2009; 2013; Hentschke and Tönnies, 2010; Hipwell et al., 2003; Kerrien et al., 1999; McLaughlin et al., 2001; 2002; 2005; Meunier et al., 1989; Miao et al., 2013; Mitrović et al., 2015; Suh et al., 2010) employ quality measurements based on pixel intensities.

Algorithms based on feature matching essentially require the definition of a specific encoding function. Regarding solely feature-based registration, the most popular approach for representing the geometry of vessels is describing them as centerline points (Dibildox et al., 2014; Feldmar et al., 1997; Groher et al., 2009; Khoo and Kapoor, 2015; Kim et al., 2014; Kita et al., 1998; Mourgues et al., 2003; Reinertsen et al., 2007; Toledo et al., 1998; Tom et al., 1994). Employing the neighborhood of points leads to a graph-based representation of the vascular structures (Charnoz et al., 2005a; 2005b; Groher et al., 2007; 2009; Robben et al., 2013; Toledo et al., 1998). But also curves can be used as a representation of vessels (Coppini et al., 1995; Liu et al., 1998). The approach by Liu et al. (1998) explicitly names the near projective invariance of tubular objects as a motivation. In a 3D-2D scenario, extracted 3D skeletons are projected and compared to 2D skeletons, using the distance as quality measure. For distance calculation, equidistant sample points are determined on one curve. Their correspondences are then identified by intersection with a line that is orthogonal to the sampled curve. Instead of collecting all centerline points, some approaches are limited to the use of bifurcation points only (Charnoz et al., 2005a; 2005b; Coppini et al., 1995; Groher et al., 2007), e.g. together with a graph structure (Charnoz et al., 2005a; 2005b; Groher et al., 2007) to store information of the vascular shape in between.

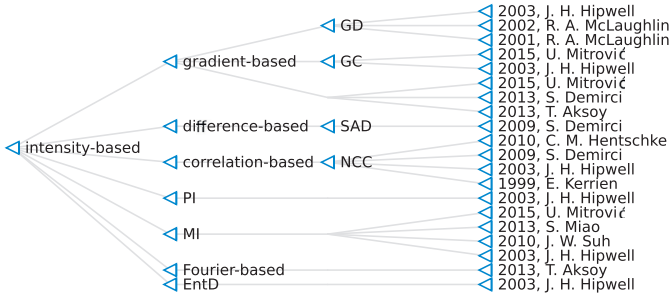

Fig. 6. Intensity-based registration: Categories: registration basis, cost function. Tags: intensity-based.

The actual distance measure depends very much on the underlying encoding function. Since most feature-based algorithms employ centerline points, the Euclidean (Dibildox et al., 2014; Groher et al., 2007; 2009; Khoo and Kapoor, 2015; Kim et al., 2014; Kita et al., 1998; Liu et al., 1998; Reinertsen et al., 2007; Tom et al., 1994) and geodesic (Coppini et al., 1995; Mourgues et al., 2003) distances are most frequently used. Representing centerline points as tensor, Feldmar et al. (1997) define a dedicated tensor distance that is minimized for aligning the projected vessel tensor and 2D image features. Charnoz et al. (2005a); 2005b) and Robben et al. (2013) use a graph matching to align the vascular trees of both input images.

Whereas feature-based methods generally require preprocessing for feature extraction and preparation, intensity-based approaches evaluate the alignment quality of images on a pixel level. As visualized in Fig. 6, typical intensity-based cost functions are Mutual Information (MI) (Hipwell et al., 2003; Miao et al., 2013; Mitrović et al., 2015; Suh et al., 2010), correlation-based measurements like Normalized Cross Correlation (NCC) (Demirci et al., 2009; Hentschke and Tönnies, 2010; Hipwell et al., 2003; Kerrien et al., 1999), Sum of Absolute Differences (SAD) (Demirci et al., 2009), Pattern Intensity (PI) (Hipwell et al., 2003) or

gradient-based cost functions such as Gradient Difference (Hipwell et al., 2003; McLaughlin et al., 2001; 2002; 2005), Gradient Correlation (Hipwell et al., 2003; Mitrović et al., 2015) and special adaptation of these (Aksoy et al., 2013; Demirci et al., 2013).

Showing the advantage of intensity-based approaches over feature-based methods, studies performed by McLaughlin et al. (2001); 2002); 2005) compared different measures for 3D-2D registration in neurovascular applications. Results indicate that the use of Gradient Difference as cost function achieves a significantly higher accuracy (1.4 mm compared to 2.3 mm) than minimizing the Euclidean distance between the projected 3D and 2D centerlines. A reason for this observation is that the feature-based algorithm is "sensitive to inaccuracies in the position of 2-D and 3-D skeletonized points" (McLaughlin et al. (2005).

Feature-based approaches are "fast and robust, but often have to cope with segmentation errors and thus lack of accuracy" (Groher et al., 2007) and the "issue of using features rather than intensities for the registration influences [the registration] method in terms of accuracy and robustness" (Groher et al., 2009). Charnoz et al. explicitly take into account segmentation errors by searching for a set of "most likely solutions which are updated along the process" (Charnoz et al., 2005b) instead of focussing on one single best match. Importing inaccuracies with segmentation of features might be restricted to a certain amount by using appropriate segmentation methods. Some authors argue that "intensity-based methods work best when there are large overlapping landmark areas, which is not a property of the vasculature" (Ruijters et al., 2009). However, intensity-based approaches "utilize all the information in the images [and therefore it is] reasonable to expect that they are more accurate than feature-based methods" Markelj et al. (2012).

Despite being the most frequently used classification, our literature analysis found that a differentiation into intensity-based and feature-based algorithms only, is not sufficient. Many authors (Groher et al., 2007; Liao et al., 2013; McLaughlin et al., 2001; Miao et al., 2011; Mitrović et al., 2013b; Vermandel et al., 2006) name "hybrid approaches" as a third group, combining elements of both intensity- and feature-based types. Hybrid registration algorithms usually "register segmentations of the (reconstructed) vasculature using intensity-based methods" (Groher et al., 2007). Taking another look at Fig. 5, intensity-based approaches largely work with images, feature-based approaches usually register two models and hybrid algorithms mainly perform a model-image registration.

As detailed in Markelj et al. (2012), aligning 3D and 2D image data involves certain transformations for bringing them into dimensional correspondence. For vessel registration, the most frequently used strategies are volume projection, e.g. maximum intensity projection (MIP) (Hentschke and Tönnies, 2010; Kerrien et al., 1999; Miao et al., 2013; Mitrović et al., 2015), Digitally Reconstructed Radiograph (DRR) (Aksoy et al., 2013; Carrell et al., 2010; Demirci et al., 2013; Hipwell et al., 2003; Liao et al., 2013; Lv et al., 2012; Metz et al., 2009a; 2009b; Miao et al., 2011; Mitrović et al., 2015; Raheem et al., 2010) and model projection. Chan and Chung (2003), Chan et al. (2004) and Lau and Chung (2006) use 3D vessels represented as a "set of spheres with the centres set to the coordinates of [vessel centerline] points, and radii equal to their [respective vessel diameter]" (Lau and Chung, 2006). Those spheres are then projected onto the image plane and the resulting binary image is compared using SSD. Many more algorithms use a model projection (Florin et al., 2005; Groher et al., 2007; 2009; 2010; Hadida et al., 2012; Jomier et al., 2006; Kim et al., 2014; Kita et al., 1998; Liao et al., 2010; Liu et al., 1998; Metz et al., 2012; Mitrović et al., 2013a; 2013b; 2015; Raheem et al., 2010; Rivest-Henault et al., 2012; Ruan et al., 1992; Ruijters et al., 2009; Sundar et al., 2006; Toledo et al., 1998; Turgeon et al., 2005).

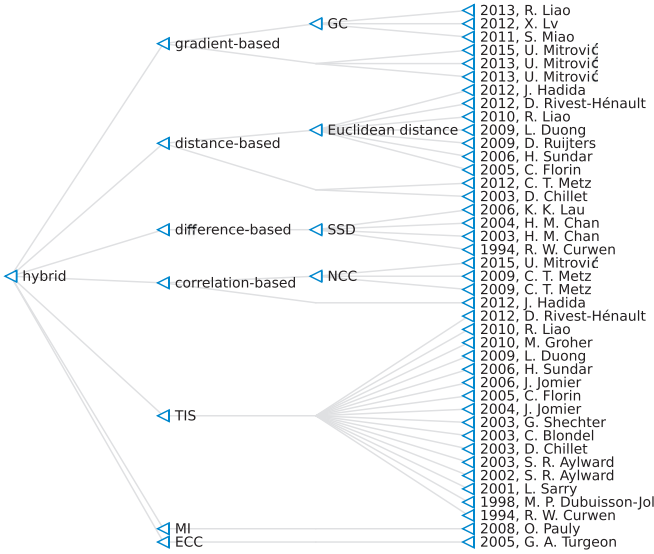

Fig. 7. Hybrid registration: Categories: registration basis, cost function. Tags: hybrid.

For registering a biplane input with a 3D point cloud using a cost function defined in 3D space, Dibildox et al. (2014) perform a reconstruction of the model to achieve dimensional correspondence and compare the performance of Gaussian Mixture Models (GMM) with the special case of a Weighted GMM and an Oriented GMM for minimizing the distance between both point clouds. More reconstruction is performed for a biplane-3D registration (Khoo and Kapoor, 2015; Rivest-Henault et al., 2012), using a single biplane sequence (Sarry and Boire, 2001), a rotational X-Ray Angiography sequence (Blondel et al., 2003) and in a 3D-2D approach (Duong et al., 2009).

Increasing the performance of quality evaluation, some authors decide to employ the computation of distance maps (Aksoy et al., 2013; Chillet et al., 2003; Demirci et al., 2009; Duong et al., 2009; Florin et al., 2005; Kim et al., 2014; Liao et al., 2010; Metz et al., 2012; Rivest-Henault et al., 2012; Ruijters et al., 2009; Sundar et al., 2006). By calculating distance maps, an "explicit establishment of point correspondences between 2D and 3D graphs can be avoided during the optimization" (Liao et al., 2010). This has certain advantages, since "the patches cannot be well matched" (Khoo and Kapoor, 2015) if a different point sampling in the respective images is used. In addition, transforming and projecting a 3D point cloud in an iterative manner on a 2D distance map allows to precompute that map once, thus greatly reducing the computational effort needed for registration.

As shown in Fig. 7, cost functions for hybrid approaches include Gradient Correlation (Liao et al., 2013; Lv et al., 2012; Miao et al., 2011), the matching of projected vessel orientations with 2D gradients (Mitrović et al., 2013a; 2013b; 2015) SSD (Chan and Chung, 2003; Chan et al., 2004; Curwen et al., 1994; Lau and Chung, 2006), cosine similarity (Hadida et al. (2012), Entropy of Correlation Coefficient (ECC) (Turgeon et al., 2005), MI (Pauly et al., 2008) and correlation-based measurements like NCC (Metz et al., 2009a; 2009b; Mitrović et al., 2015). However, the majority of hybrid algorithms is summing up intensities in a target image (Aylward et al., 2002; 2003; Blondel et al., 2003; Chillet et al., 2003; Curwen et al., 1994; Dubuisson-Jolly et al., 1998; Duong et al., 2009; Florin et al., 2005; Groher et al., 2010; Jomier and Aylward, 2004; Jomier et al., 2006; Liao et al., 2010; Rivest-Henault et al., 2012; Sarry and Boire, 2001; Shechter et al., 2003; Sundar et al., 2006). We define this very popular measure as Target Intensity Sum (TIS). Some authors choose to compute a distance map on the target image in order to

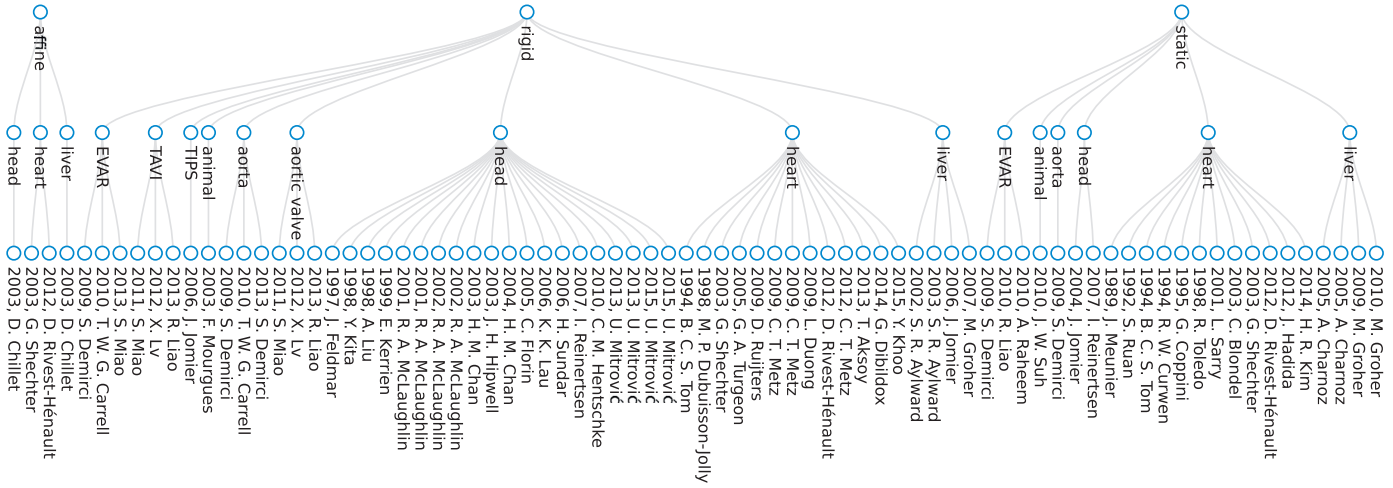

Fig. 8. Application and Deformation: Most approaches are rigid. Categories: global geometric transformation, application. Tags: none.

further speed up optimization and use the sum of distance values at projected model points (Chillet et al., 2003; Duong et al., 2009; Florin et al., 2005; Liao et al., 2010; Rivest-Henault et al., 2012; Ruijters et al., 2009; Sundar et al., 2006).

4.2. Application and deformation

Splitting algorithms based on their registration basis is just one option to differentiate related literature. Categorizing algorithms by application makes it much easier to choose the right approach for a specific medical procedure. The characteristics of vasculature and its surroundings greatly differ between patients, but also among different regions of the body. Whereas cerebral vasculature is of smaller size and subjected to minimal motion, the aorta is of much larger size and coronary arteries move along with the beating heart.

Many algorithms are designed for specific vasculature of one anatomical region only. Hence, an application of these for a different purpose will most likely yield variations in accuracy and precision. Algorithms associating details of the aortic shape to a specific cost function (Liao et al., 2013) cannot be employed for registering liver vessels. Similar, algorithms registering the liver's hepatic and portal trees (Aylward et al., 2003) might not be suited for TAVI procedures requiring a matching of the ascending aorta and its main coronary branches. Furthermore, almost all approaches (even if designed for general use) are tested for single applications only, i.e. there is no proof that an algorithm performs well under completely different circumstances. Certain applications require additional properties of the transformation. A registration method intended for applications in the vicinity of the heart has to take into account sinusoidal motion, while algorithms for neurointerventional use mainly work with smaller static vasculature.

Categorizing algorithms in either rigid or local deformable geometric transformation helps choosing the desired approach. Rigid vessel registration is used in applications registering the descending (Carrell et al., 2010; Demirci et al., 2013; Miao et al., 2013) as well as ascending aorta (Liao et al., 2013; Lv et al., 2012; Miao et al., 2011), coronary arteries (Aksoy et al., 2013; Dibildox et al., 2014; Dubuisson-Jolly et al., 1998; Duong et al., 2009; Khoo and Kapoor, 2015; Metz et al., 2009a; 2009b; 2012; Rivest-Henault et al., 2012; Ruijters et al., 2009; Shechter et al., 2003; Tom et al., 1994; Turgeon et al., 2005), in liver applications (Aylward et al., 2002; 2003; Groher et al., 2007; Jomier et al., 2006) and for neurointerventional applications (Chan and Chung, 2003; Chan et al., 2004; Chillet et al., 2003; Feldmar et al., 1997; Florin et al., 2005; Hentschke and Tönnies, 2010; Hipwell et al., 2003; Jomier and Aylward, 2004; Kerrien et al., 1999; Kita et al., 1998; Lau and Chung, 2006; Liu et al., 1998; McLaughlin et al., 2001; 2002; 2005; Mitrović et al., 2013a; 2013b; 2015; Reinertsen et al., 2007; Sundar et al., 2006).

As depicted in Fig. 8, despite the vast majority of rigid registration algorithms, some approaches employ affine transformations using normal brain and liver vasculature (Chillet et al., 2003) or keep the global transformation fixed (static). Splines are the most popular schemes used for interpolation and natural smoothing of a deformable registration (Demirci et al., 2009; Mitra et al., 2011). As most deformation schemes require an initialization that is close to the optimum position, some authors chose to perform first a rigid and then a local deformable registration (Demirci et al., 2009; Reinertsen et al., 2007; Tom et al., 1994).

Performing subsequently rigid, affine and local deformations of coronary arteries is done by Shechter et al. (2003) with B-splines to express the local deformation and by Rivest-Henault et al. (2012) employing the concept of thin plate splines (TPS) and an additional energy term enforcing a certain smoothness of the overall deformation. B-splines are also used on coronary arteries (Blondel et al., 2003; Curwen et al., 1994; Toledo et al., 1998) and TPS are used by Reinertsen et al. (2007) for the correction of brain shift, by Raheem et al. (2010) for endovascular repair of abdominal aortic aneurysms and by Kim et al. (2014) for coronary registration. Groher et al. (2010) use TPS together with a length preserving term for registering liver images and ensure additional smoothness using a diffusion regularization term (Groher et al., 2009). A length preservation is also used by Shechter et al. (2003), by Liao et al. (2010) together with a smoothness term for EVAR and by Sarry and Boire (2001) registering the coronary arteries with a 3D contour model using Fourier shape descriptors.

Another common way to express local deformation is using a displacement field, e.g. for quantification of abdominal aortic deformation after EVAR (Demirci et al., 2009), for registering the portal and hepatic liver trees by formulating a tree matching problem that yields a deformation vector field for each tree node Charnoz et al. (2005a); 2005b), using an optical flow approach for accessing biaxial deformation of the epicardial surface (Meunier et al., 1989) or motion of the coronary arteries (Ruan et al., 1992; Tom et al., 1994). A displacement field can also be combined with additional smoothness terms (Demirci et al., 2009). Blondel et al. (2003) ensure a certain smoothness of their coronary arteries by minimizing the spatial gradient of the tensor product of

B-splines in three dimensions and a time dimension. Jomier and Aylward (2004) combine linear transformations in a hierarchical approach and other algorithms use a planispheric deformation model (Hadida et al., 2012) or spherical harmonics (Coppini et al., 1995) for registering coronary arteries. Finally, animal data are used for registration in a rigid (Mourgues et al., 2003) and a deformable approach using a B-spline-based Free Form Deformation together with a hierarchical control point grid (Suh et al., 2010).

4.3. Modality, dimensionality and validation

The visibility of vascular structures can be enhanced using contrast agent or specific modalities like Time of Flight (ToF) MRA. Hence, a further splitting of algorithms within the modality category, into contrasted and non-contrasted image acquisition contributes to a better differentiation of the literature. As shown in Fig. 9, CTA, MRA and DSA or X-Ray Angiography clearly dominate this domain. Still, many more modalities exist for preoperative diagnosis and interventional imaging and these are also employed for vessel-based registration. Referring only to the inherent (physical) imaging technique is rather vague, since various modalities come with different dimensionalities. MRA can be acquired in 3D, but also in 2D, US is usually 2D, but the 3D and 4D counterpart receives growing interest, especially in obstetric ultrasonography for diagnosis (Merz and Abramowicz, 2012). IVUS and OCT usually still refer to the 2D variant, but higher dimensions are possible. Consequently, adding a description of the exact dimension to the used modality is necessary. As depicted in Fig. 10, most algorithms perform a 3D-2D registration and are tested with clinical data. However, this could also indicate that clinical tests were evaluated in the respective publications only.

CTA is mainly used as the 3D component within 3D-2D registration to 2D X-Ray Angiography (Aksoy et al., 2013; Demirci et al., 2013; Duong et al., 2009; Hadida et al., 2012; Kim et al., 2014; Lv et al., 2012; Metz et al., 2009b; Ruijters et al., 2009) and DSA (Carrell et al., 2010; Groher et al., 2007; 2009; 2010; Kim et al., 2014; Liao et al., 2010; 2013; McLaughlin et al., 2001; Miao et al., 2011). Some of these algorithms are tested with clinical data (Carrell et al., 2010; Demirci et al., 2013; Groher et al., 2007; 2009; Hadida et al., 2012; Kim et al., 2014; Liao et al., 2013; Lv et al., 2012; Metz et al., 2009b; Miao et al., 2011; Ruijters et al., 2009) or with synthetic data (Duong et al., 2009; Groher et al., 2010; Hadida et al., 2012; Liao et al., 2010; Ruijters et al., 2009). Aksoy et al. (2013) evaluate their algorithm on clinical data, synthetic data and a phantom model. Since “ground truth for real patient data is difficult to obtain” (Liao et al., 2010), synthesized and natural transformations and deformations are applied to an extracted vessel tree and projected onto the 2D image plane. It should be noted that the “advantage of using the simulated instead of real 2D projections is that we have the ground truth and hence can validate our registration accuracy in 3D” (Liao et al., 2010). McLaughlin et al. (2001) designed a dedicated phantom model for measuring the accuracy of CTA-DSA and also MRA-DSA registration. For obtaining a ground truth, fiducial markers were positioned around the model. Not every publication specifies an exact input modality and authors claim that their registration works with any preoperatively acquired model of the aorta (Liao et al., 2013; Lv et al., 2012; Miao et al., 2011). If clinical data are used, ground truth is often created by manually selected correspondences (Miao et al., 2013).

Aside from mono-plane approaches, CTA is also registered to biplane X-Ray Angiography (e.g. two Angiographic images acquired at the same time from nearly orthogonal viewpoints) (Dibildox et al., 2014; Khoo and Kapoor, 2015; Rivest-Henault et al., 2012) and using a sequence of 3D CTA images, CTA is registered to a 2D X-Ray Angiography sequence (Metz et al., 2009a; 2012).

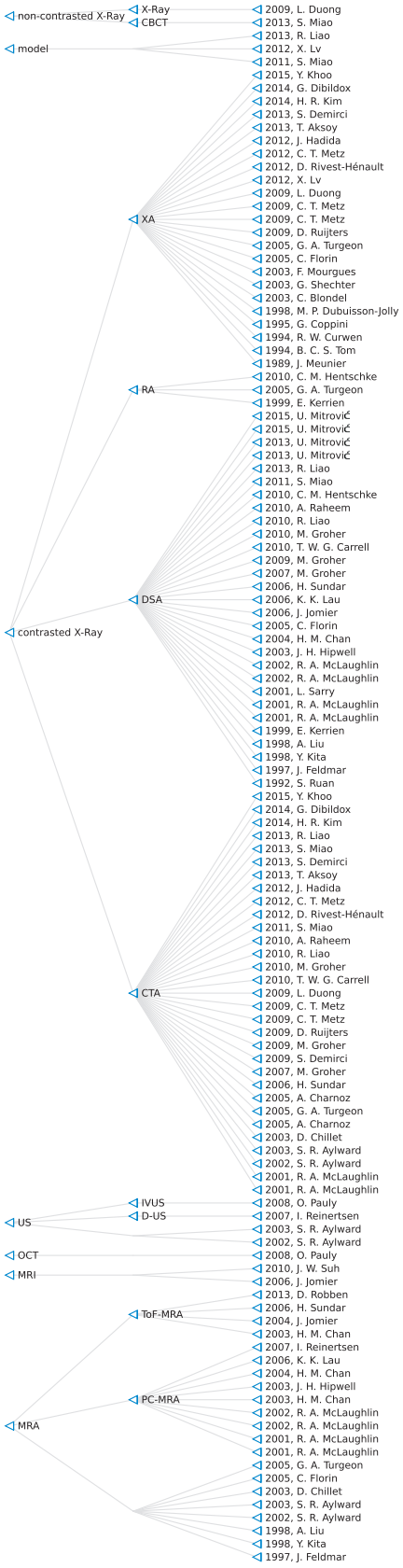

Fig. 9. Modalities: Categories: modality. Tags: none.

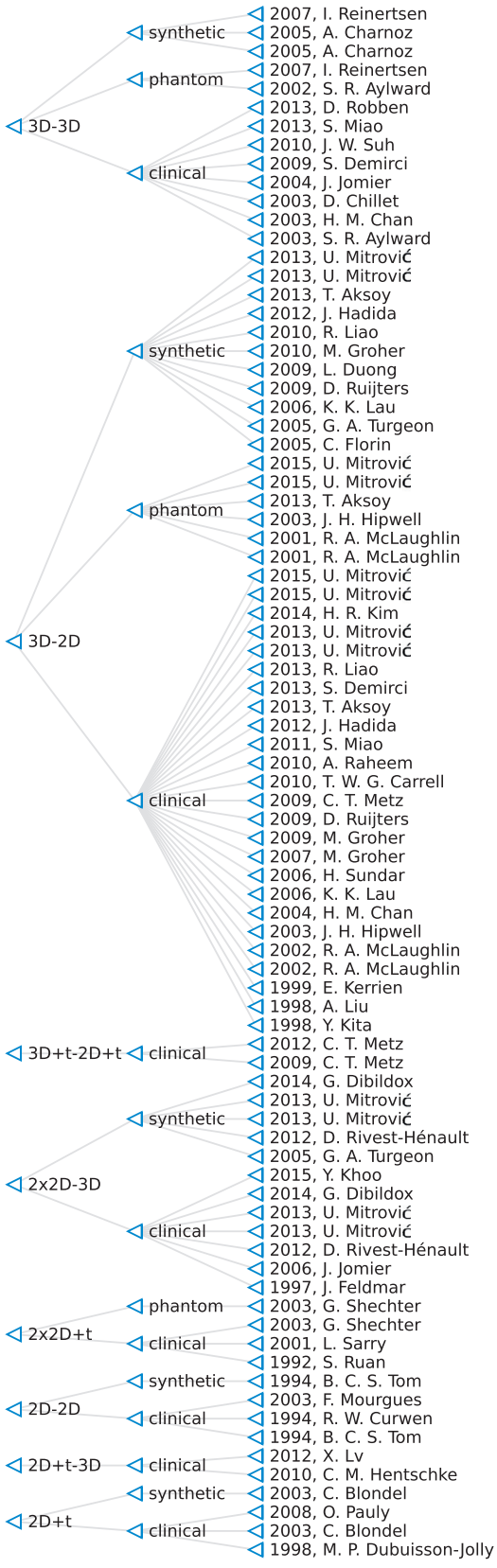

Fig. 10. Validation: Most algorithms are validated with clinical data. Categories: dimensionality, validation. Tags: none.

All these algorithms are tested with clinical data or additionally with synthetic data (Dibildox et al., 2014; Rivest-Henault et al., 2012). CTA is also registered to a normal 2D X-Ray employing the contrast provided by the outline of a radiopaque guide wire (Duong et al., 2009) and to clinical non-contrasted Cone Beam CT (CBCT) (Miao et al., 2013), making use of the segmented spine by thresholding the Hounsfield Units and thereby starting with a rough alignment.

Besides mono-modal registration (Chillet et al., 2003), MRA is involved in 3D-3D registration with CTA (Chillet et al., 2003) and in 3D-2D registration with DSA (Kita et al., 1998; Liu et al., 1998) and biplane DSA (Feldmar et al., 1997). Similar PC-MRA is registered to 3D Doppler-US (Reinertsen et al., 2007), 3D ToF-MRA (Chan and Chung, 2003) and 2D DSA (Chan et al., 2004; Hipwell et al., 2003; Lau and Chung, 2006; McLaughlin et al., 2001; 2002). In addition, ToF-MRA registration is employed for intrasubject monitoring purposes and thereby registered to another ToF-MRA acquisition of the same patient (Jomier and Aylward, 2004; Robben et al., 2013). Sundar et al. (2006) do not explicitly name DSA, but their algorithm digitally subtracts a reference fluoroscopy image acquired before contrast injection from a contrast-injected image to obtain segmented blood vessels. Both, clinical ToF-MRA and CTA data are then registered with 2D Fluoroscopy. In general, MR-based approaches are validated on clinical (Chan and Chung, 2003; Chan et al., 2004; Chillet et al., 2003; Feldmar et al., 1997; Jomier and Aylward, 2004; Jomier et al., 2006; Kita et al., 1998; Lau and Chung, 2006; Liu et al., 1998; McLaughlin et al., 2002; Robben et al., 2013; Sundar et al., 2006), phantom (Hipwell et al., 2003; McLaughlin et al., 2001; Reinertsen et al., 2007) and synthetic datasets (Lau and Chung, 2006; Reinertsen et al., 2007).

Chillet et al. (2003) use an atlas-based algorithm to register CTA using liver data and MRA using data of the head. A vascular atlas based on distance maps is formed for each modality. The registration process is tested with extracted centerlines from clinical data and simulations with different offsets and rotations are performed. The portal and the hepatic liver system are registered with this approach and also arteriovenous malformations in the head can be detected by comparing each voxel with respective mean and standard deviation. Another statistical approach by Robben et al. (2013) labels the Circle of Willis using statistical atlas- and graph-based registration with ToF-MRA volumes of the head, but an exact deformation is not calculated. Clinical tests are also performed on MRI data of animals (Suh et al., 2010) and for registration of MRI and 2D DSA during a TIPS procedure (Jomier et al., 2006).

In order to have more realistic data, a surgery simulator for simulating liver and vascular system deformations was used by Charnoz et al. (2005a); 2005b) to create a synthetic tree model. This was then randomly pruned losing up to 40% of its branches to simulate segmentation errors. 600 test cases with different deformations and different pruning were evaluated.

Turgeon et al. (2005) try to register preoperative ECG-gated CTA, MRA or RA to intraoperative monoplane as well as biplane X-Ray Angiograms. Realistic synthetic datasets are simulated from a 4D human heart dataset. The 3D-biplane registration performed much better than the 3D-2D tests. In addition, a 3D-3D registration was implemented using a reconstruction of the biplane input leading to practically the same accuracy than their 3D-biplane approach. Aylward et al. (2002) try to augment 3D intraoperative US with preoperative CTA or MRA volumes by mainly using a homemade phantom and continue their approach Aylward et al. (2003), registering CTA to CTA by using liver data and also MRA to MRA using pre-treatment, post-radiation therapy, and post-surgery head MRA clinical data.

Clinical pre- and postoperative EVAR CTA data are registered deformably by Demirci et al. (2009) and a 3D Rotational

Angiography to 2D DSA registration of the head is performed rigidly by Kerrien et al. (1999) and using a DSA sequence to accumulate intensities over time by Hentschke and Tönnies (2010). Raheem et al. use a CTA volume together with interventional DSA and X-Ray Angiography, with the latter being the mask image of the DSA. A registration for AAA procedures is done using the mask image and the CTA assuming a rigid relationship with the vertebra. Then six manually chosen point pairs are defined in the DSA and used to achieve a TPS-based deformation of the aorta. After that, the segmented and deformed aorta is registered rigidly. The authors assume that "the main cause of deformation is the stiff interventional instruments, and that once one of these instruments is inserted the deformation will remain reasonably constant" (Raheem et al., 2010).

Florin et al. (2005) register X-Ray Angiography to 3D MRA and 3D DSA. Motion reconstruction of coronary arteries is achieved with a biplane sequence of DSA images (Ruan et al., 1992; Sarry and Boire, 2001) and with a biplane X-Ray Angiography sequence (Coppini et al., 1995; Shechter et al., 2003). Mitrović et al. use 3D DSA of the head for registration with 2D DSA (Mitrović et al., 2015) and biplane DSA (Mitrović et al., 2013a; 2013b). Blondel et al. (2003) use a single rotational X-Ray Angiography sequence for creating a 4D reconstruction of coronary arteries, Curwen et al. (1994), Meunier et al. (1989) and Tom et al. (1994) use two consecutive frames of an X-Ray Angiography sequence to infer the coronary motion in 2D, Dubuisson-Jolly et al. (1998) track a point on a single polyline representing a coronary vessel in 2D and Mourgues et al. (2003) try to overlay a manually reconstructed coronary tree model on intraoperative X-Ray Angiography using manually defined point correspondences. Those approaches are tested using clinical data (Blondel et al., 2003; Curwen et al., 1994; Dubuisson-Jolly et al., 1998; Mitrović et al., 2013a; 2013b; 2015; Mourgues et al., 2003; Ruan et al., 1992; Sarry and Boire, 2001; Shechter et al., 2003; Tom et al., 1994), a phantom (Mitrović et al., 2015; Shechter et al., 2003) and synthetic data (Blondel et al., 2003; Florin et al., 2005; Mitrović et al., 2013a; 2013b; Tom et al., 1994).

Finally, there are some approaches proposing image registration involving IVUS. Aligning IVUS and OCT sequences, the method proposed by Pauly et al. (2008) is rather based on vessel lumen instead of dealing with tubular objects or complete vessel trees. The lumen is segmented in both input modalities and then a statistical shape space with vectors describing the lumen contour is created. Different filters are used to create those features and the algorithm's output is a matching of corresponding image pairs. The matching is intended as a preprocessing step for image fusion, which could then register the single pairs.

4.4. Optimization

As already stated, there are great differences between the used cost functions, depending very much on the registration basis of a particular approach. While intensity-based algorithms are considered more accurate and precise than feature-based approaches, they are computationally more expensive and therefore mostly inefficient. Still, the computational effort can be decreased dramatically when advanced optimization strategies are used. If an underlying continuous function can be broken down into discrete samples, many optimization schemes exist that lead to faster convergence. Chan and Chung (2003) and Chan et al. (2004) use Powell's conjugate direction method to iteratively search for the minimum value of the SSD along each of the six degrees of freedom using Brent's method. If the discrete image or volume is too large and an exhaustive search is not feasible, downsampling images in a pyramid with multiple levels using a multi-resolution strategy can reduce processing time (Dubuisson-Jolly et al., 1998; Groher et al., 2010; Lau and Chung, 2006; Liao et al., 2013; Lv et al., 2012; McLaughlin et al., 2001; 2002; Metz et al., 2009a; 2009b; Miao et al., 2011; 2013). It has been reported that a multi-resolution approach seems to "facilitate the searching to the adjacent local minima, rather than to transcend the local minima" (Lau and Chung, 2006). Therefore, Lau and Chung also use a "systematic multi-start-point approach combined with a local optimization method (Powell's method)" (Lau and Chung (2006), which helps finding the global optimum. Another possibility to speed up the search on image intensities is using integral images (Mitrović et al., 2013a; 2013b; 2015).

In case of deformable registration, deformations are usually not specified for each single pixel for efficiency reasons. Common approaches include using B-Splines and TPS expressing a deformation field. While B-Splines are embedded in a regular grid with control points, TPS can be used together with a smoothing parameter to control the rigidity of the resulting deformation, which can be meaningful when using vascular structures. B-Splines can be easily optimized using a multi-level approach, e.g. Suh et al. (2010) use an FFD based on B-Splines with multiple levels and different control point spacings for each level.

Probabilistic and stochastic approaches can facilitate the search for local and global optima. Evolutionary algorithms, such as genetic population (Jomier et al., 2006; Rivest-Henault et al., 2012; Ruijters et al., 2009), are considered as a strategy that is "less likely to get stuck in a local optimum" (Ruijters et al., 2009). A cost function consisting of the "sum of the Gaussian-blurred intensity values in the [DSA] at the projected model points" (Jomier et al., 2006) is optimized using a genetic algorithm optimizer. Other authors "use the Condensation form of sequential Monte Carlo sampling to estimate a cost function gradient" (Florin et al., 2005) for finding the global minimum. Besides, the Kalman filter is successfully adopted (Curwen et al., 1994; Feldmar et al., 1997; Toledo et al., 1998).

Many more strategies are tested or used during registration, e.g. Newton's method (Liu et al., 1998), Powell's method (Lau and Chung, 2006; Mitrović et al., 2013a; 2013b; 2015; Rivest-Henault et al., 2012; Ruijters et al., 2009), Nelder-Mead (Downhill-Simplex) (Demirci et al., 2013; Groher et al., 2007; Rivest-Henault et al., 2012; Turgeon et al., 2005), gradient descent (Florin et al., 2005; Groher et al., 2009; 2010; Hentschke and Tönnies, 2010; Hipwell et al., 2003; Khoo and Kapoor, 2015; Metz et al., 2009a; 2009b; Rivest-Henault et al., 2012; Shechter et al., 2003; Sundar et al., 2006), Greedy Search (Robben et al., 2013), dynamic programming (Blondel et al., 2003; Tom et al., 1994) and Least Squares (Feldmar et al., 1997; Liu et al., 1998; Lv et al., 2012; Reinertsen et al., 2007). One can employ the special case of Least Trimmed Squares to "reduce the number of outliers in the [ICP-based] point matching procedure" (Reinertsen et al., 2007). The Broyden–Fletcher–Goldfarb–Shanno algorithm is used (Aksoy et al., 2013; Groher et al., 2009; 2010; Liao et al., 2010) as well as another nonlinear optimization, the Fletcher-Reeves-Polak-Ribière variant of the conjugate gradient method (Blondel et al., 2003; Sarry and Boire, 2001). It has been declared important to test many different optimization techniques before choosing the best or a combination of various methods. Rivest-Henault et al. (2012) have tested nine different global or local optimization strategies including a direct approach and a population-based stochastic method as global optimizers and many local optimizers like Best Neighbor, Nelder-Mead, Powell's and Brent's method.

Occlusions and dissimilarities induced by varying presence of contrasted vessels and medical instruments can cause severe problems during image registration (Demirci et al., 2008; 2013). Additional objects in the image can have adverse effects on vascular segmentation. On the other hand, they also distract intensity-based registration optimizations from the real global optimum, since occlusions are usually not present in both input modali-

ties. A special disocclusion technique is proposed for an approach that "first initiates a reconstruction of the occluded image part, given an outline of the occluded region, and then performs a 2D-3D registration of the reconstructed 2D image and the 3D pre-operative volume employing a gradient-based similarity measure" (Demirci et al., 2013).

For estimating the rotational parameters of a rigid transformation, Aksoy et al. compare DRRs with X-Ray Angiography images "in Fourier domain due to its translation invariance and robustness against noise [and] occlusions. In a second step, 3D translation is recovered in spatial domain by minimizing the distance of the 3D vessel model to the 2D vessels" (Aksoy et al., 2013) using distance maps.

Instead of completely separating translation and rotation, Kerrien et al. use a two-step process which first calculates the translation by maximizing the cross correlation of two images and assuming a small rotation then "recovers the residual rigid-body motion [using] a modified optical flow technique" (Kerrien et al., 1999). The minimization criteria of Kita et al. is "initially only based on rotation by separating out the translation effect" (Kita et al., 1998) and although "the correct position and posture of the model is not obtained at once, because of inaccurate matching pairs and linearization errors [in the rotation matrix], the 3D model quickly converges to the correct state by iterating the point matching and model transformation processes" (Kita et al., 1998). In order to avoid local minima (e.g. caused by optimizing rotational parameters that are far from the actual transform), Duong et al. and Sundar et al. split the registration in two steps, performing an optimization "only for the translational parameters which allows the initial guess to be refined" (Sundar et al., 2006), "followed by a second run of optimization on [all six rigid body] parameters" (Duong et al., 2009).

Similar, after an initial parameter guess based on C-arm pose, Mitrović et al. first "reduce possibly large in-plane translation errors [comparing] a DRR projection of the 3D binary vessel tree centerlines and the 2D image [and in a second step evaluate four registration methods] which involve the optimization of 3D image's rigid-body and C-arm's parameters" (Mitrović et al., 2015).

To further speed up the registration process, high-quality projections of the 3D image data or volume can be calculated in a separate preparation step. The actual matching process can then be performed much more efficiently. This is of particular interest for interventional registration tasks, for which real-time processing is a clinical requirement. Here, 3D data are usually extracted from a pre-interventional patient scan that is acquired at least a couple of days (exact numbers depend on the specific country's medical care system) before the actual intervention, justifying the division into preparation and matching phases. Aksoy et al. (2013) propose to prepare various DRR projections sampled from different viewpoints as templates. These are then compared to the target image during the matching phase.

Khoo and Kapoor (2015) register a 3D CTA model with X-Ray Angiography images for percutaneous coronary interventions. The algorithm uses two point sets and tries to simultaneously solve for pose and correspondences. A convex relaxation of the original non-convex optimization problems is proposed. The program is extended using feature-descriptors consisting of the coordinates of neighborhood points around each single point to optimize point correspondences. The approach does a rigid registration and one intention is to provide a high quality starting point for following registration algorithms.

Finally, a transfer of computations to the graphics processing unit (GPU) can accelerate the processing time by a large extent. Intensity-based approaches work with single pixels and thus the computation of cost functions becomes computationally expensive. DRR projections used to compare a volume with a 2D image often "remain the dominant processing component of the registration algorithm" (Hipwell et al., 2003). However, the computation can be ported to the GPU in order to overcome that drawback, making intensity-based registrations much faster. A few approaches (Demirci et al., 2013; Liao et al., 2013; Lv et al., 2012; Metz et al., 2009a; 2009b; Miao et al., 2011; Mitrović et al., 2015; Turgeon et al., 2005) make use of GPUs, all of them using a rigid deformation model and mainly a hybrid registration basis.

Four of these approaches are intended for the aorta, using Gradient Correlation as the cost function and CTA and a contrasted X-Ray as input. Demirci et al. (2013) employ a single render pass together with a transfer function for conversion from Hounsfield units to X-Ray attenuation to compute the DRR. Liao et al. (2013) and Miao et al. (2011) create a DRR from the segmented aorta model and the coronary ostia only and match it to a pre-filtered DSA image. "It takes about 15 ms to generate 256 $\times$ 256 DRRs from a 256 $\times$ 256 $\times$ 256 volume with an NVIDIA Quadro FX 360M" (Miao et al., 2011) and in a second publication "10 ms ... with an NVIDIA Quadro FX 580M" (Liao et al., 2013). (Lv et al., 2012) extend the approach by Miao et al. (2011) registering the 3D input model to a sequence of X-Ray Angiography images. First, the image frame with the largest amount of contrast being visible, is used for rigid registration employing the approach by Miao et al. (2011). Within the same motion cycle, the motion is estimated based on an optical flow analysis. The resulting transformation estimation for each frame is then refined more precisely and a motion model is updated. More heart cycles are subsequently registered, using B-Spline interpolation of neighboring rigid transformations from the motion model instead of the flow analysis, because other cycles have less contrast, i.e. the contrast is fading out.

Three more GPU-based approaches register coronary arteries. Metz et al. (2009b) explicitly use a CTA-derived polygon mesh of segmented vasculature and render a DRR, linearly approximating the accumulated X-Ray attenuation in a fragment shader program utilizing OpenGL. A DRR is also rendered on the GPU using a coronary lumen model by Metz et al. (2009a). Turgeon et al. create a binary model projection using "on-screen renderings by the NVIDIA GeForce FX 5900 graphic card through the use of VTK and OpenGL libraries" (Turgeon et al., 2005).

Finally, a very recent approach by Mitrović et al. registers 3D and 2D DSA images of the head using multiple registration algorithms. "The tested methods were implemented in CUDA and executed on NVidia GTS 450 GPU from MATLAB (The MathWorks, Inc., USA) on Intel(R) Core(TM) i7 CPU 860 @ 2.80 GHz machine with 8 GB system memory" (Mitrović et al., 2015).

5. Discussion

Compared to the conventional review paper paradigm, which is typically static w.r.t. the chosen categorization, benefits of our proposed living review visualization tool include flexible adaptation of the classification scheme and the possibility to perform complete individual searches. Queries on the underlying algorithm database can for instance be performed with different combinations of categories defined in Section 2 and the displayed results can be arbitrarily narrowed down to further specific selections. Besides providing individual overviews of available algorithms, the living review allows a more in-depth analysis of specific aspects that may not be apparent otherwise. By exploring the references discussed in this paper according to different categorizations, we made several interesting observations which will be discussed in the following.

As indicated in Fig. 11, almost all algorithms in the database perform intrasubject registration of images acquired from the same patient. Only a couple of intersubject algorithms exist that aim

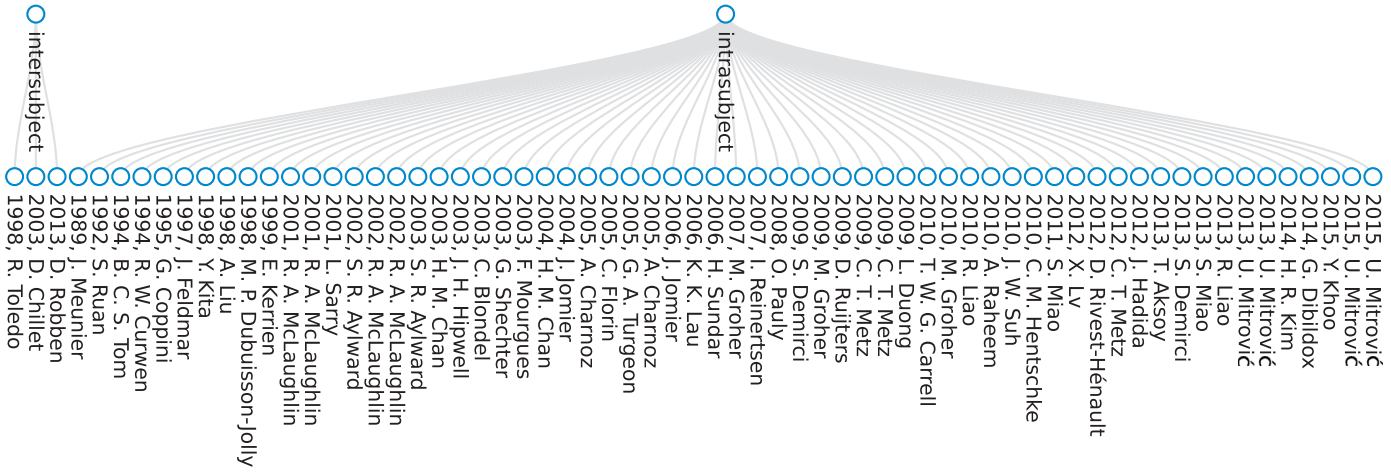

Fig. 11. Subject: Two different registration types are tagged. Categories: subject. Tags: none.

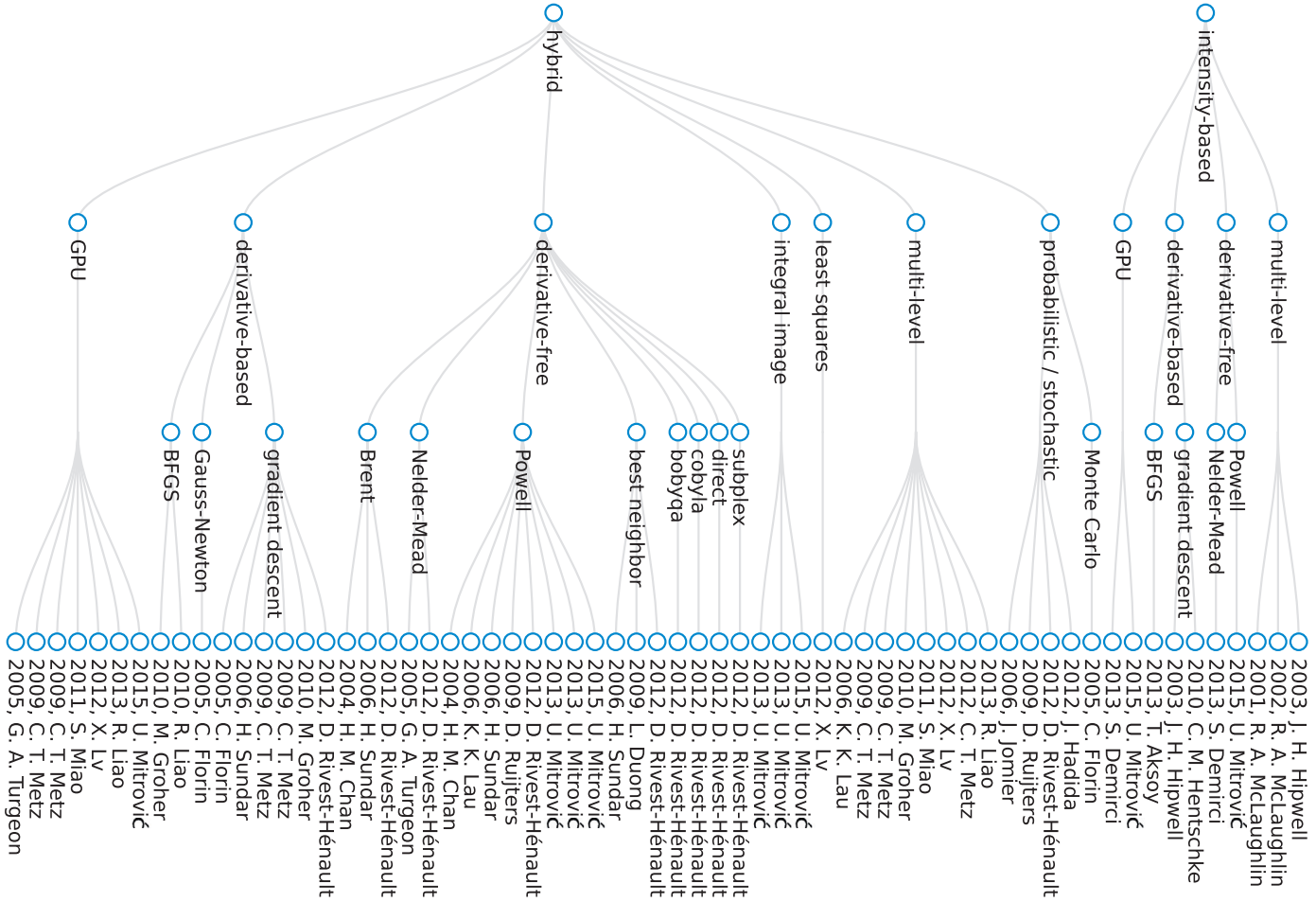

Fig. 12. Multiple tree layers: A more specific search. Hybrid or intensity-based algorithms having both a 3D and a 2D component are visualized. Categories: registration basis, dimensionality, optimization. Tags: hybrid, intensity-based, 3D-2D, 3D+t-2D+t, 2D+t-3D, 2x2D-3D.

at building up vascular atlases (Chillet et al., 2003; Toledo et al., 1998) or guiding intersubject label transfer (Robben et al., 2013). One natural reason for researchers concentrating on intrasubject registration might be grounded in the complex validation requirements for intersubject approaches. As mentioned before, each individual's vascular structures are considered unique and, hence, building up an atlas requires availability of large amount of image data and appropriate storage facilities.

Observing the distribution of algorithms within the registration basis in Fig. 5, another striking effect becomes apparent. Features and intensity-based cost functions have been more and more combined to form hybrid measures throughout the past decades. Interestingly, despite being incredibly popular in general medical image analysis (Aljabar et al., 2012), machine-learning approaches have not yet entered the field of vascular image registration. Machine-learning algorithms usually also need a training

set, hence a limited availability of medical data might redirect the focus to other approaches. Furthermore, intersubject approaches might provide great opportunities and could be investigated more.

As mentioned in Section 2.1, algorithms are not tested on the same hardware and the runtime as well as some very subjective categories like required level of user interaction are not included in our review. In addition, it has to be noted that used datasets differ a lot in quality and quantity. A tag indicating validation with public databases seems advisable, but respective databases are usually not mentioned in analyzed vessel registration papers and most authors do not compare their algorithm to existing ones in terms of performance. "To motivate further development and validation of 3D-2D registration methods" (Mitrović et al., 2015), a few publications make their validation images available online (Mitrović et al., 2013a; 2015). A link to the used data is provided and the data can be downloaded.

The tree in Fig. 12 displays selected 3D-2D registration approaches employing hybrid and intensity-based cost functions only. We can see that many different optimization strategies are used. Since hybrid or intensity-based approaches often calculate a projection of the 3D data, GPU-based optimization is feasible and recommended. However, only a few publications actually describe this step.

Promising achievements for general medical image registration employing GPU computation power (Kubias et al., 2008; Moulik and Boonn, 2011; Tornai et al., 2012) give hope that a similar application in the vessel registration domain could yield dramatic improvement.

As indicated above, new algorithms should also include more tests with existing algorithms using a common dataset or specific public databases. Common datasets do not only provide a foundation for meaningful comparisons, they could be also used for differentiation into normal vasculature and those differing because of diseases as well as vasculature heavily occluded by medical devices.

Future work regarding the visualization will include more tags and additional information like impact factors of each paper. As suggested by our reviewers, visualization strategies integrating a weighting of certain categories should be investigated and natural language processing might lead towards a more supervised classification.

6. Conclusion

This paper contributes to a better differentiation of vessel registration techniques by analyzing relevant literature in a flexible way. An intuitive user interface for displaying the data is provided, allowing the user to find a query-specific visualization. As mentioned in the beginning, depending on the user's personal preferences, a particular discrimination of the data can be rather intuitive or not. Our visualization does not require a certain differentiation and users can create their individual trees according to their specific needs.

Last but not least, we cordially invite other researchers to contribute to the proposed database fostering future research in the field of vascular registration techniques. This invitation is accompanied by the hope that the living review paradigm serves as a role model for other living reviews and thus spreads to other fields of research.

References

Aksoy, T., Unal, G., Demirci, S., Navab, N., Degertekin, M., 2013. Template-based CTA to x-ray angio rigid registration of coronary arteries in frequency domain with automatic x-ray segmentation. Med. Phys. 40 (10), 101903.

Aljabar, P., Wolz, R., Rueckert, D., 2012. Manifold Learning for Medical Image Registration, Segmentation, and Classification. IGI Global.

Astola, J., Virtanen, I., 1982. Entropy Correlation Coefficient, a Measure of Statistical Dependence for Categorized Data. University of Vaasa, Finland.

Aylward, S.R., Jomier, J., Guyon, J.-P., Weeks, S., 2002. Intra-operative 3D ultrasound augmentation. In: IEEE International Symposium on Biomedical Imaging: Nano to Macro (ISBI), 2002. IEEE, pp. 421–424.

Aylward, S.R., Jomier, J., Weeks, S., Bullitt, E., 2003. Registration and analysis of vascular images. Int. J. Comput. Vis. 55 (2-3), 123–138.

Blondel, C., Malandain, G., Vaillant, R., Devernay, F., Coste-Manière, E., Ayache, N., 2003. 4-D tomographic representation of coronary arteries from one rotational X-Ray sequence. In: Medical Image Computing and Computer-Assisted Intervention - MICCAI 2003. In: Lecture Notes in Computer Science, 2878. Springer, pp. 416–423.

Brent, R.P., 1971. An algorithm with guaranteed convergence for finding a zero of a function. Comput. J. 14 (4), 422–425.

Buzug, T.M., Weese, J., Fassnacht, C., Lorenz, C., 1996. Using an entropy similarity measure to enhance the quality of DSA images with an algorithm based on template matching. In: Visualization in Biomedical Computing. Springer, pp. 235–240.

Buzug, T.M., Weese, J., Fassnacht, C., Lorenz, C., 1997. Image registration: convex weighting functions for histogram-based similarity measures. In: CVRMed-MRCAS'97. Springer, pp. 203–212.

Carrell, T.W.G., Modarai, B., Brown, J.R.I., Penney, G.P., 2010. Feasibility and limitations of an automated 2D-3D rigid image registration system for complex endovascular aortic procedures. J. Endovasc. Ther. 17 (4), 527–533.

Chan, H.-M., Chung, A.C.S., 2003. Efficient 3D-3D vascular registration based on multiple orthogonal 2D projections. In: Biomedical Image Registration. In: Lecture Notes in Computer Science, 2717. Springer, pp. 301–310.

Chan, H.M., Chung, A.C.S., Yu, S.C.H., Wells, W.M.I.I.I., 2004. 2D-3D vascular registration between digital subtraction angiographic (DSA) and magnetic resonance angiographic (MRA) images. In: IEEE International Symposium on Biomedical Imaging: From Nano to Macro (ISBI), 2004. IEEE, pp. 708–711.

Charnoz, A., Agnus, V., Malandain, G., Forest, C., Tajine, M., Soler, L., 2005. Liver registration for the follow-up of hepatic tumors. In: Medical Image Computing and Computer-Assisted Intervention MICCAI 2005. In: Lecture Notes in Computer Science, 3750. Springer, pp. 155–162.

Charnoz, A., Agnus, V., Malandain, G., Nicolau, S., Tajine, M., Soler, L., 2005. Design of robust vascular tree matching: validation on liver. In: Information Processing in Medical Imaging. In: Lecture Notes in Computer Science, 3565. Springer, pp. 443–455.

Chillet, D., Jomier, J., Cool, D., Aylward, S., 2003. Vascular atlas formation using a vessel-to-image affine registration method. In: Medical Image Computing and Computer-Assisted Intervention–MICCAI 2003. In: Lecture Notes in Computer Science, 2878. Springer, pp. 335–342.

Coppini, G., Demi, M., Marraccini, P., L'Abbate, A., 1995. 3-D heart motion from X-Ray angiography. In: Computers in Cardiology 1995. IEEE, pp. 71–74.

Crow, F.C., 1984. Summed-area tables for texture mapping. ACM SIGGRAPH Comput. Graph. 18 (3), 207–212.

Curwen, R., Amini, A., Duncan, J., Lee, F., 1994. Tracking vascular motion in X-ray image sequences with Kalman snakes. In: Computers in Cardiology 1994. IEEE, pp. 109–112.

Demirci, S., Baust, M., Kutter, O., Manstad-Hulaas, F., Eckstein, H.-H., Navab, N., 2013. Disocclusion-based 2D–3D registration for aortic interventions. Comput. Biol. Med. 43 (4), 312–322.

Demirci, S., Kutter, O., Manstad-Hulaas, F., Bauernschmitt, R., Navab, N., 2008. Advanced 2D-3D registration for endovascular aortic interventions: addressing dissimilarity in images.

Demirci, S., Manstad-Hulaas, F., Navab, N., 2009. Quantification of abdominal aortic deformation after EVAR. In: Proceedings of SPIE. SPIE Digital Library.72611U–72611U–9

Dibildox, G., Baka, N., Punt, M., Aben, J.-P., Schultz, C., Niessen, W., van Walsum, T., 2014. 3D/3D registration of coronary CTA and biplane XA reconstructions for improved image guidance.

Dubuisson-Jolly, M.-P., Liang, C.-C., Gupta, A., 1998. Optimal polyline tracking for artery motion compensation in coronary angiography. In: Computer Vision, 1998. Sixth International Conference on. IEEE, pp. 414–419.

Duong, L., Liao, R., Sundar, H., Tailhades, B., Meyer, A., Xu, C., 2009. Curve-based 2D-3D registration of coronary vessels for image guided procedure. In: Proceedings of SPIE. SPIE Digital Library.72610S–72610S–10

Feldmar, J., Malandain, G., Ayache, N., Fernndez-Vidal, S., Maurincomme, E., Trousset, Y., 1997. Matching 3D MR angiography data and 2D X-ray angiograms. In: CVRMed-MRCAS'97. In: Lecture Notes in Computer Science, 1205. Springer, pp. 129–138.

Florin, C., Williams, J., Khamene, A., Paragios, N., 2005. Registration of 3D angiographic and X-Ray images using sequential Monte Carlo sampling. In: Computer Vision for Biomedical Image Applications. In: Lecture Notes in Computer Science, 3765. Springer, pp. 427–436.

Groher, M., Baust, M., Zikic, D., Navab, N., 2010. Monocular deformable model-to-image registration of vascular structures. In: Biomedical Image Registration. In: Lecture Notes in Computer Science, 6204. Springer, pp. 37–47.

Groher, M., Jakobs, T.F., Padoy, N., Navab, N., 2007. Planning and intraoperative visualization of liver catheterizations: new CTA protocol and 2D-3D registration method. Acad. Radiol. 14 (11), 1325–1340.

Groher, M., Zikic, D., Navab, N., 2009. Deformable 2D-3D registration of vascular structures in a one view scenario. IEEE Trans. Med. Imaging 28 (6), 847–860.

Hadida, J., Desrosiers, C., Duong, L., 2012. Stochastic 3D motion compensation of coronary arteries from monoplane angiograms. In: Medical Image Computing and Computer-Assisted Intervention MICCAI 2012. In: Lecture Notes in Computer Science, 7510. Springer, pp. 651–658.
Hentschke, C.M., Tönnies, K.D., 2010. Automatic 2D-3D registration of cerebral DSA data sets. In: Bildverarbeitung für die Medizin. Springer, pp. 162–166.
Hipwell, J.H., Penney, G.P., McLaughlin, R.A., Rhode, K., Summers, P., Cox, T.C., Byrne, J.V., Noble, J.A., Hawkes, D.J., 2003. Intensity-based 2-D-3-D registration of cerebral angiograms. IEEE Trans. Med. Imaging 22 (11), 1417–1426.
Jomier, J., Aylward, S.R., 2004. Rigid and deformable vasculature-to-image registration: a hierarchical approach. In: Medical Image Computing and Computer-Assisted Intervention MICCAI 2004. In: Lecture Notes in Computer Science, 3216. Springer, pp. 829–836.
Jomier, J., Bullitt, E., Van Horn, M., Pathak, C., Aylward, S.R., 2006. 3D/2D model–to-image registration applied to TIPS surgery. In: Medical Image Computing and Computer-Assisted Intervention MICCAI 2006. In: Lecture Notes in Computer Science, 4191. Springer, pp. 662–669.
Kerrien, E., Berger, M.-O., Maurincomme, E., Launay, L., Vaillant, R., Picard, L., 1999. Fully automatic 3D/2D subtracted angiography registration. In: Medical Image Computing and Computer-Assisted Intervention MICCAI99. In: Lecture Notes in Computer Science, 1679. Springer, pp. 664–671.
Khoo, Y., Kapoor, A., 2015. Towards non-iterative closest point: exact recovery of pose for rigid 2D/3D registration using semidefinite programming. arXiv preprint arXiv:1501.00630.
Kim, H.-R., Kang, M.-S., Kim, M.-H., 2014. Non-rigid registration of vascular structures for aligning 2D X-ray angiography with 3D CT angiography. In: Advances in Visual Computing. In: Lecture Notes in Computer Science, 8887. Springer, pp. 531–539.
Kita, Y., Wilson, D.L., Noble, J.A., 1998. Real-time registration of 3D cerebral vessels to X-ray angiograms. In: Medical Image Computing and Computer-Assisted Intervention MICCAI98. In: Lecture Notes in Computer Science, 1496. Springer, pp. 1125–1133.
Krabbe-Hartkamp, M.J., Van der Grond, J., De Leeuw, F.E., De Groot, J.C., Algra, A., Hillen, B., Breteler, M.M., Mali, W.P., 1998. Circle of Willis: morphologic variation on three-dimensional time-of-flight MR angiograms.. Radiology 207 (1), 103–111.
Kubias, A., Deinzer, F., Feldmann, T., Paulus, D., Schreiber, B., Brunner, T., 2008. 2D/3D image registration on the GPU. Pattern Recognit. Image Anal. 18 (3), 381–389.
Lau, K.K., Chung, A.C.S., 2006. A global optimization strategy for 3D-2D registration of vascular images.. In: British Machine Vision Conference (BMVC), pp. 489–498.
Lesage, D., Angelini, E.D., Bloch, I., Funka-Lea, G., 2009. A review of 3D vessel lumen segmentation techniques: models, features and extraction schemes. Med. Image Anal. 13 (6), 819–845.
Liao, R., Miao, S., Zheng, Y., 2013. Automatic and efficient contrast-based 2-D/3-D fusion for trans-catheter aortic valve implantation (TAVI). Comput. Med. Imaging Graph. 37 (2), 150–161.
Liao, R., Tan, Y., Sundar, H., Pfister, M., Kamen, A., 2010. An efficient graph-based deformable 2D/3D registration algorithm with applications for abdominal aortic aneurysm interventions. In: Medical Imaging and Augmented Reality. In: Lecture Notes in Computer Science, 6326. Springer, pp. 561–570.
Liu, A., Bullitt, E., Pizer, S.M., 1998. 3D/2D registration via skeletal near projective invariance in tubular objects. In: Medical Image Computing and Computer-Assisted Intervention MICCAI98. In: Lecture Notes in Computer Science, 1496. Springer, pp. 952–963.
Lv, X., Liao, R., Liu, Y., Miao, S., 2012. A framework for automatic, accurate, and fast 2-D+T/3-D registration applied to trans-catheter aortic valve implantation (TAVI) procedures. In: IEEE International Symposium on Biomedical Imaging: From Nano to Macro (ISBI), 2012. IEEE, pp. 956–959.
Maes, F., Collignon, A., Vandermeulen, D., Marchal, G., Suetens, P., 1997. Multimodality image registration by maximization of mutual information. IEEE Trans. Med. Imaging 16 (2), 187–198.
Maintz, J.B.A., Viergever, M.A., 1998. A survey of medical image registration. Med. Image Anal. 2 (1), 1–36.
Markelj, P., Tomaževič, D., Likar, B., Pernuš, F., 2012. A review of 3D/2D registration methods for image-guided interventions. Med. Image Anal. 16 (3), 642–661.
McLaughlin, R.A., Hipwell, J., Hawkes, D.J., Noble, J.A., Byrne, J.V., Cox, T., 2002. A comparison of 2D-3D intensity-based registration and feature-based registration for neurointerventions. In: Medical Image Computing and Computer-Assisted Intervention MICCAI 2002. In: Lecture Notes in Computer Science, 2489. Springer, pp. 517–524.
McLaughlin, R.A., Hipwell, J., Hawkes, D.J., Noble, J.A., Byrne, J.V., Cox, T.C., 2005. A comparison of a similarity-based and a feature-based 2-D-3-D registration method for neurointerventional use. IEEE Trans. Med. Imaging 24 (8), 1058–1066.
McLaughlin, R.A., Hipwell, J., Penney, G.P., Rhode, K., Chung, A., Noble, J.A., Hawkes, D.J., 2001. Intensity-based registration versus feature-based registration for neurointerventions. Proc. Med. Image Underst. Anal..
Merz, E., Abramowicz, J.S., 2012. 3D/4D ultrasound in prenatal diagnosis: is it time for routine use? Clin. Obstet. Gynecol. 55 (1), 336–351.
Metz, C., Schaap, M., Klein, S., Neefjes, L., Capuano, E., Schultz, C., van Geuns, R., Serruys, P., van Walsum, T., Niessen, W., 2009. Patient specific 4D coronary models from ECG-gated CTA data for intra-operative dynamic alignment of CTA with X-ray images. In: Medical Image Computing and Computer-Assisted Intervention MICCAI 2009. In: Lecture Notes in Computer Science, 5761. Springer, pp. 369–376.
Metz, C., Schaap, M., Klein, S., Rijnbeek, P., Neefjes, L., Mollet, N., Schultz, C., Serruys, P., Niessen, W., van Walsum, T., 2012. Alignment of 4D coronary CTA with monoplane X-ray angiography. In: Augmented Environments for Computer-Assisted Interventions. In: Lecture Notes in Computer Science, 7264. Springer, pp. 106–116.
Metz, C., Schaap, M., Klein, S., Weustink, A., Mollet, N., Schultz, C., van Geuns, R., Serruys, P., van Walsum, T., Niessen, W., 2009. GPU accelerated alignment of 3-D CTA with 2-D X-ray data for improved guidance in coronary interventions. In: 2009. ISBI'09. IEEE International Symposium on Biomedical Imaging: from Nano to Macro. IEEE, pp. 959–962.
Meunier, J., Bourassa, M., Bertrand, M., Verreault, M., Mailloux, G., 1989. Regional epicardial dynamics computed from coronary cineangiograms. In: Computers in Cardiology 1989, Proceedings.. IEEE, pp. 307–310.
Miao, S., Liao, R., Pfister, M., Zhang, L., Ordy, V., 2013. System and method for 3-D/3-D registration between non-contrast-enhanced CBCT and contrast-enhanced CT for abdominal aortic aneurysm stenting. In: Medical Image Computing and Computer-Assisted Intervention MICCAI 2013. In: Lecture Notes in Computer Science, 8149. Springer, pp. 380–387.
Miao, S., Liao, R., Zheng, Y., 2011. A hybrid method for 2-D/3-D registration between 3-D volumes and 2-D angiography for trans-catheter aortic valve implantation (TAVI). In: IEEE International Symposium on Biomedical Imaging: From Nano to Macro (ISBI), 2011. IEEE, pp. 1215–1218.
Mitra, J., Marti, R., Oliver, A., Lladó, X., Vilanova, J.C., Meriaudeau, F., 2011. A comparison of thin-plate splines with automatic correspondences and B-splines with uniform grids for multimodal prostate registration. In: Proceedings of SPIE. SPIE Digital Library.79642T–79642T
Mitrović, U., Pernuš, F., Likar, B., Špiclin, Ž., 2015. Simultaneous 3D-2D image registration and C-arm calibration: application to endovascular image-guided interventions. Med. Phys. 42 (11), 6433–6447.
Mitrović, U., Špiclin, Ž., Likar, B., Pernuš, F., (2013a). 3D-2D registration of cerebral angiograms: a method and evaluation on clinical images. IEEE Trans. Med. Imaging 32 (8), 1550–1563.
Mitrović, U., Špiclin, Ž., Likar, B., Pernuš, F., (2013b). Method for 3D-2D registration of vascular images: application to 3D contrast agent flow visualization. In: Clinical Image-Based Procedures. From Planning to Intervention. In: Lecture Notes in Computer Science, 7761. Springer, pp. 50–58.
Moulik, S., Boonn, W., 2011. The role of GPU computing in medical image analysis and visualization. In: Proceedings of SPIE, 7967. SPIE Digital Library.7967L–7967L
Mourgues, F., Vieville, T., Falk, V., Coste-Manière, E., 2003. Interactive guidance by image overlay in robot assisted coronary artery bypass. In: Medical Image Computing and Computer-Assisted Intervention – MICCAI 2003. In: Lecture Notes in Computer Science, 2878. Springer, pp. 173–181.
Nelder, J.A., Mead, R., 1965. A simplex method for function minimization. Comput. J. 7 (4), 308–313.
Pauly, O., Unal, G., Slabaugh, G., Carlier, S., Fang, T., 2008. Semi-automatic matching of OCT and IVUS images for image fusion. In: Proceedings of SPIE. International Society for Optics and Photonics. SPIE Digital Library.69142N–69142N–11
Penney, G.P., Weese, J., Little, J., Desmedt, P., Hill, D.L.G., Hawkes, D.J., et al., 1998. A comparison of similarity measures for use in 2-D-3-D medical image registration. IEEE Trans. Med. Imaging 17 (4), 586–595.
Peters, T.M., Cleary, K. (Eds.), 2008, Image-guided Interventions, Technology and Applications. Springer.
Powell, M.J.D., 1964. An efficient method for finding the minimum of a function of several variables without calculating derivatives. Comput. J. 7 (2), 155–162.
Raheem, A., Carrell, T., Modarai, B., Penney, G., 2010. Non-rigid 2D-3D image registration for use in endovascular repair of abdominal aortic aneurysms. In: Medical Image Understanding and Analysis, pp. 153–157.
Reinertsen, I., Descoteaux, M., Siddiqi, K., Collins, D.L., 2007. Validation of vessel-based registration for correction of brain shift. Med. Image Anal. 11 (4), 374–388.
Rivest-Henault, D., Sundar, H., Cheriet, M., 2012. Nonrigid 2D/3D registration of coronary artery models with live fluoroscopy for guidance of cardiac interventions. IEEE Trans. Med. Imaging 31 (8), 1557–1572.
Robben, D., Sunaert, S., Thijs, V., Wilms, G., Maes, F., Suetens, P., 2013. Anatomical labeling of the circle of willis using maximum a posteriori graph matching. In: Medical Image Computing and Computer-Assisted Intervention MICCAI 2013. In: Lecture Notes in Computer Science, 8149. Springer, pp. 566–573.
Ruan, S., Bruno, A., Collorec, R., Coatrieux, J., 1992. 3D motion and reconstruction of coronary networks. In: Engineering in Medicine and Biology Society, 1992 14th Annual International Conference of the IEEE, 5. IEEE, pp. 2048–2049.
Ruijters, D., ter Haar Romeny, B.M., Suetens, P., 2009. Vesselness-based 2D3D registration of the coronary arteries. Int. J. Comput. Assist. Radiol. Surg. 4 (4), 391–397.
Sarry, L., Boire, J.-Y., 2001. Three-dimensional tracking of coronary arteries from biplane angiographic sequences using parametrically deformable models. IEEE Trans. Med. Imaging 20 (12), 1341–1351.
Shechter, G., Devernay, F., Coste-Manière, E., Quyyumi, A., McVeigh, E.R., 2003. Three-dimensional motion tracking of coronary arteries in biplane cineangiograms. IEEE Trans. Med. Imaging 22 (4), 493–503.
Suh, J.W., Scheinost, D., Qian, X., Sinusas, A.J., Breuer, C.K., Papademetris, X., 2010. Serial nonrigid vascular registration using weighted normalized mutual information. In: IEEE International Symposium on Biomedical Imaging: From Nano to Macro, 2010. IEEE, pp. 25–28.

Sundar, H., Khamene, A., Xu, C., Sauer, F., Davatzikos, C., 2006. A novel 2D-3D registration algorithm for aligning fluoro images with 3D Pre-op CT/MR images. In: Proceedings of SPIE. SPIE Digital Library.61412K–61412K

Toledo, R., Radeva, P., Von Land, C., Villanueva, J., 1998. 3D dynamic model of the coronary tree. In: Computers in Cardiology 1998. IEEE, pp. 777–780.

Tom, B., Efstratiadis, S., Katsaggelos, A., 1994. Motion estimation of skeletonized angiographic images using elastic registration. IEEE Trans. Med. Imaging 13 (3), 450–460.

Tornai, G.J., Cserey, G., Pappas, I., 2012. Fast DRR generation for 2D to 3D registration on GPUs. Med. Phys. 39 (8), 4795–4799.

Turgeon, G.-A., Lehmann, G., Guiraudon, G., Drangova, M., Holdsworth, D., Peters, T., 2005. 2D-3D registration of coronary angiograms for cardiac procedure planning and guidance. Med. Phys. 32 (12), 3737–3749.

Vermandel, M., Betrouni, N., Gauvrit, J.-Y., Pasquier, D., Vasseur, C., Rousseau, J., 2006. Intrinsic 2D/3D registration based on a hybrid approach: use in the radiosurgical imaging process.. Cell. Mol. Biol. 52 (6), 44–53.

Weese, J., Penney, G.P., Desmedt, P., Buzug, T.M., Hill, D.L.G., Hawkes, D.J., 1997. Voxel-Based 2-D/3-D registration of fluoroscopy images and CT scans for image-guided surgery. IEEE Trans. Inf. Technol. Biomed. 1 (4), 284–293.

Wells, W.M., Viola, P., Atsumi, H., Nakajima, S., Kikinis, R., 1996. Multi-modal volume registration by maximization of mutual information. Med. image Anal. 1 (1), 35–51.

World Health Organization, 2015. Factsheet No317. http://www.who.int/mediacentre/factsheets/fs317/en/, Retrieved: 05/05/2015.